Viability of Hydrogen Isotopes Separation via Heterolytic Dissociation–Driven Chemical Affinity Quantum Sieving on Inexpensive Alkali–Earth Oxides †

Simone Puricelli,‡ Giovanna Bruno,‡ Carlo Gatti,¶ Alessandro Ponti,*,¶ and Massimo Mella*,‡

Dipartimento di Scienza ed Alta Tecnologia, Università degli Studi dell'Insubria, via Valleggio 11, 22100 Como (I), and Istituto di Scienze e Tecnologie Chimiche "Giulio Natta" – SCITEC, Consiglio Nazionale delle Ricerche, via Camillo Golgi 19, 20133 Milano (I)

E-mail: alessandro.ponti@scitec.cnr.it; massimo.mella@uninsubria.it

†Authors' Contributions: (SP) electronic structure calculations, results analysis and interpretation; (GB) electronic structure calculations, results analysis, interpretation and writing; (CG) results analysis and interpretation; (AP) electronic structure calculations, results analysis and interpretation, writing; (MM) conceptualization, electronic structure calculations, results analysis and interpretation, supervision, writing.

*To whom correspondence should be addressed

‡Uninsubria

¶SCITEC–CNR

Abstract

The quest for economically viable strategies to separate hydrogen molecule isotopologues has recently provided clear indications on the design principles that ought to be implemented to satisfy the growing request for deuterium and tritium homodimers. In this respect, we investigate by electronic structure calculations whether easily obtainable, environmentally respectful, and inexpensive alkali–earth oxides may be suitable materials when it comes to separating hydrogen isotopologues. We found that hydrogen dimers heterolytically dissociate upon chemisorption on the most reactive three–coordinated vertex Mg, Ca, Sr and O sites, the formed species remaining in close proximity due to a strong H^+/H^- interaction. The inclusion of quantum zero point motion in the description of the adsorption energetics, mandatory if one wishes to differentiate the isotopologues behavior, indicated that the chemisorption energy becomes more negative the heavier the isotope involved. Isotopic selectivities estimated via Ideal Adsorbed Solution Theory (IAST) appear orders of magnitude higher than those previously presented. As chemisorbed species may catalyze an exchange reaction with gaseous molecules hinging on their nature as Broensted acid and Lewis base, we searched for possible processes competing with the desorption of vicinal adsorbed species; our results suggest that production of heterodimers (e.g. HD) is unlikely.

Keywords

Hydrogen isotopes, adsorption, chromatographic separation

1 Introduction

The scientific and industrial importance of the heavier hydrogen isotopes has been steadily growing over the last decades. This trend descends from their usage as neutron moderators, in nonradioactive isotope tracing of (e.g.) drug metabolites, in the study of chemical mechanisms, as well as in the determination of the hydrogen position in organic molecules.

Eventually, D_2 and T_2 may also sustain nuclear fusion reactors as feedstock fuels for the production of more sustainable and cleaner energy. Therefore, it comes at no surprise that attention has being payed to develop cost– and energy–effective isotope separation methods. Among the ones available today, it is worth mentioning cryogenic distillation,[1] Gilder sulfide process, and thermal cycling adsorption process.[2] In spite of their general usefulness, the low separation factor afforded by the mentioned processes descending from the very similar physicochemical properties of the species involved, juxtaposed with the high energy consumption often due to very low operational temperatures, represents a serious limitation to a more widespread production of purer heavy hydrogen isotopes.

Starting from the observations made by Bennakker *et al*[3] basing on the dependence of quantum effects on the species mass, alternative processes have begun to attract attention. In the end, one may attempt to harness in her/his favor the higher probability of quantum tunnelling in the case of lighter species,[4–8] the lower de Broglie wavelength (which reduces the effect on the kinetic energy of a particle when the latter becomes progressively more localized) of heavier species,[9,10] or the different impact of the zero–point energy due to mass effect when molecules are surface adsorbed.[11–13] So far, the last two possibilities have generated two approaches respectively named Kinetic Quantum Sieving (KQS) and Chemical Affinity Quantum Sieving (CAQS). While in the former one exploits primarily a different mass–related effective molecular size descending from Heisenberg's uncertainty principle by selecting 3D materials or 2D membranes with pores of diameter capable of excluding the lighter species, the second hinges on the fact that adsorption energies becomes more negative the heavier the isotope is. As a consequence, the gas–surface partition constant follows the order $T_2 > D_2 > H_2$. As an example, we mention that Cu(I)–exchanged zeolites appear to have a selectivity toward D_2 of 24.9 at 70 K.[14]

As for the more general context of CAQS, different material types have been investigated with the hope of finding a few instances in which high selectivity and low cost come simultaneously. Thus, metal organic framework (MOF) derived materials (especially when they

afford open metal sites, OMS's, capable of coordinating X_2,[15–34] with X=H, D, T), ion–exchanged zeolites,[14,35–41] metal organic cage (MOCs)[42] or simpler organic cage[43] based materials derived from organic macrocycles, and flexible porous materials[44–48] have seen their adsorption and separation properties measured. In a few instances, selectivities sufficiently high to be exploited for industrial purposes have been found. This notwithstanding, the materials cost, their limited capacity, as well as the fact that molecules have to "be queued" to enter and leave the inner cavities of porous solids still limit a more widespread application.

Considering that many of the CAQS active materials exploit interactions between X_2 and OMS's with bond enthalpies in the 9–17 kcal/mol range, the latter being due to the formation of a nearly covalently bound metal ion–X_2 moiety,[14,15,35–37,49–52] one may speculate whether high surface area materials, which are used as adsorbents, may be employed for the same purpose of separating isotopes as the porous ones. Materials that are simultaneously inexpensive, abundant, easily regenerable, and presenting isotope–dependent adsorption energies to allow for a high selectivity must be sought. It is also important that adsorption is sufficiently strong to increase the operation temperature as close to room temperature as possible. In this respect, the literature on molecular hydrogen adsorption on group II metal oxides,[53–66] as well as our own experience on studying processes induced by the latter,[67–71] indicates the usage of such systems as stationary phases for a chemisorption–related chromatographic separation of isotopologues as tentatively viable. The latter method would be advantageous as it could be operated in a "pulse–like" fashion, the inert carrier gas extracting from the column isotopes at different elution times, instead than in a "batch–like" style desorbing the most strongly bound species to recover it.

We have thus selected to theoretically study the thermodynamics and kinetics of X_2 adsorption on Mg, Ca, Sr oxides on clusters of various sizes to model specific defective sites known to be present on their surfaces. The goal is to establish whether sufficiently large difference in adsorption properties between isotopologues ought to be expect; the latter could

be exploited for separation purposes. Information on eventual energy barrier separating the gas phase species from the chemisorbed counterparts would also help in better define the time scales of the two fundamental processes involved. Important for our objective, it is the fact that many researchers have suggested the adsorption of the hydrogen molecule to lead to the heterolytic cleavage of the H_2 bond,[61–63,66,72,73] with the two fragments still remaining in strong interaction due to the opposite charge.[57] This means, in turn, that six stiff vibrational modes may characterize the molecule adsorbed state, and that the impact on their frequencies (i.e. of the zero–point energy) due to the change in isotope mass ought to be substantial. Besides, the close proximity between H^+ and H^- suggested by both experimental results and the occasional theoretical data may be key in limiting isotopic scrambling with gas phase molecules.

In the end, we have found that all three alkali–earth oxides studied may be employed for the separation of hydrogen isotopes. However, better performances ought to be expected from MgO primarily due to the presence of stiffer vibrational modes for the adsorbed species. In spite of this, the heavier oxides may allow to use a higher operational temperature due to their more negative chemisorption energy for the various species. In the end, a compromise may need to be stricken in selecting the stationary phase and operational conditions that reduce the production cost for mass unit of, e.g., D_2. We also found that barriers sufficiently high to impede scrambling process are indeed present if one considers a gas phase molecule impinging on the chemisorbed species on the sites we have explored.

The outline of our manuscript is as it follows. Section 2 describe in some details the theoretical methodologies employed in our study. Section 3 presents and discusses our computational results, confronting them with previous literature data. For the sake of organization, results regarding the thermodynamics of molecular adsorption are discussed first, and they follow an order dictated by the cation atomic number. Our attempt of rationalizing differences in behavior between the studied oxides is presented subsequently, preceding the discussion of kinetics aspects relevant for the adsorption and isotopic scrambling process.

Finally, Section 4 presents our conclusions together with an additional discussion relating previous literature data and their relevance for the general aim of this work.

2 Methods

Gas phase electronic structure calculations were carried out employing the Gaussian09[74] and Gaussian16[75] suite of programs and using the B3LYP density functional[76,77] to describe correlation and exchange energies. The basis sets used were the 6-31++G(d,p) set for the H, C, O, Mg and Ca atoms, and the dgdzvp set for the Sr atom. Similar levels of theory have been previously found able to rationalize changes in catalyst activity upon changing the metal ion involved,[78,79] and to semi-quantitatively describe intermolecular interactions between charged species.[80–83] Selected cases were also reinvestigated using a larger basis set (e.g. 6–311++G(2d,2p)) and a different functionals (i.e. DSD–BLYP) to verify the robustness of our results; these data are reported as Supporting Information.

The reactive sites for all oxides were modelled extending, as needed, a previously used model for the M3C or O3C vertex sites (M=Mg, Ca or Sr) on the MgO, CaO and SrO oxides;[69] depending on the specific information required, we switched between the minimalistic model $M_{10}O_{10}$ and two larger counterparts, namely $M_{12}O_{12}$ and $M_{16}O_{16}$, for all oxide clusters involved in the adsorption processes. This was done in order to minimize the effects on the adsorption energetics due to possible over–polarization of the molecules when the process takes place in the close vicinity of corner (M3C or O3C) or edge (M4C or O4C) sites.[67,84] *De facto*, we deemed necessary to extend a single edge of the $M_{10}O_{10}$ cluster turning it into $M_{16}O_{16}$ only to make sure that a sufficiently long distance was present between the adsorbed ionic species and the cluster boundaries. The differences found between these two cases, however, do not substantially change the overall picture provided by the smallest clusters. $M_{12}O_{12}$ was instead used to model the adsorption on M5C and O5C sites located on the face of oxides. Figure 1 provide a visual representation of the three model clusters.

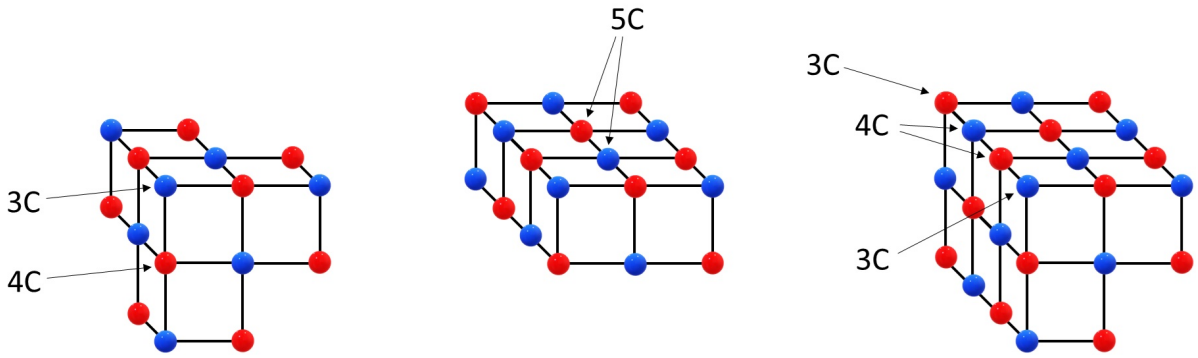

Figure 1: Structures of the three cluster models employed in electronic structure calculations: $M_{10}O_{10}$, left; $M_{12}O_{12}$, center; $M_{16}O_{16}$, right. The location of the vertex (3C), edge (4C), and face (5C) sites are also indicated.

The geometrical parameters of the MgO (cubic, $d_{MgO} = 2.1084$ Å), CaO (cubic, $d_{CaO} = 2.406$ Å[85]), and SrO (cubic, $d_{SrO} = 2.586$ Å[86]) clusters were kept frozen in all calculations, as minor effects would be expected for them[84] and for energetic quantities. This notwithstanding, adsorption energetics on 3C sites was also tested by relaxing their structure, the data being discussed partially in the main text, and, in more detail, in the Supporting Information. Putative structures for energy minima and TS's were built using data from our previous works or published articles, the geometries for reactants, products and, if needed, transition states (TS's) being fully optimized and characterized by means of frequency calculations over the unconstrained degrees of freedom of the adsorbed molecule. The latter quantities are needed to correct the adsorption energetics of the different isotopologues adding the zero point energy (ZPE) to the electronic energies, which are identical for all diatomics involved within the framework of the Born–Oppenheimer approximation. Thus, we estimated the adsorption energies as:

$$E^{ads}_{X_2} = E^{ZPE}_{MO\text{–}X_2} - E^{ZPE}_{X_2} - E_{MO} \quad (1)$$

where $E^{ZPE}_{A} = E^{ele}_{A} + ZPE_A$, E^{ele} is the electronic energy of the optimized geometries, and ZPE is the harmonic zero point energy correction. The validity of the harmonic oscillator approximation in defining the 0 K energetics was tested evaluating the magnitude of the

anharmonic corrections in a subset of relevant cases. Notice that ZPE does not include the contribution of the translational kinetic energy, the relevant degrees of freedom not being considered quantized, and that the contribution due to the rotational kinetic energy of the diatomic molecules is taken as zero (at T = 0 K molecules are in the rotational ground state). This means, in turn, that five more degrees of freedom contribute to the ZPE of the adsorbed diatomic molecules, the net effect of which would be to decrease the vibrationally corrected adsorption energy compared to the electronic counterpart. For a direct comparison between reactions taking place over different oxides, the common energy zero represented by gas phase reactants and isolated clusters was chosen. With this choice, the relative energetic positioning of intermediates and TS's can be straightforwardly used to analyze the materials relative performances.

In order to rationalise the results obtained with electronic structure methods, especially with respect to their dependence on the specific oxide and reactive sites on the surface, we decomposed the electronic adsorption energies into atomic contributions within the Quantum Theory of Atoms in Molecules (QTAIM)[87] using the Multiwfn 3.8 program package[88] (see Section 2 of Supporting Information for further details). In our approach, the atomic contributions of a generic atom A (E_A^{ads}) and fragment F (E_F^{ads}) to the total adsorption energy were calculated by simply computing:

$$E_A^{ads} = E_A^P - E_A^R \tag{2}$$

$$E_F^{ads} = \sum_{n=1}^{N} (E_{A_n}^P - E_{A_n}^R) \tag{3}$$

where E_A^P is the energy of atom A in the chemisorbed product, and E_A^R the energy of atom A in the two reagents. We also define the adsorption energy contribution of oxide bulk as the sum of all atomic contributions except those of the chemisorbed hydrogens and the related

reactive atoms on the oxide surface (Equation 4)

$$E^{ads}_{bulk} = \sum_{n=1}^{N-4} E^{P}_{A_n} - \sum_{n=1}^{N-2} E^{R}_{A_n} \quad \text{with } A_n \neq H \text{ and reactive metal or oxygen sites on oxide's surface.} \tag{4}$$

Importantly, we notice that atom energies are estimated scaling the numerical values obtained via atomic basin integration with the correction $\gamma = -\langle\hat{V}\rangle/\langle\hat{T}\rangle - 1$, which accounts for the non–fully geometrically optimized nature of our species assuming an uniform impact of the virial of external forces on all atoms (also, *vide* Section 2 in the Supporting Information). For the sake of clarity and easiness of reading, we have opted to discuss the majority of QTAIM results in the Supporting Information.

To estimate the zero pressure (i.e. assuming isolated adsorbed molecules) isotope selectivity for the sites/oxides at the temperature T, we have employed the following relation:[13]

$$S(X_2/H_2, T) = \left(\frac{m_{H_2}}{m_{X_2}}\right)^{3/2} \frac{Q_{H_2}(T)}{Q_{X_2}(T)} \exp[-(E^{ZPE}_{X_2} - E^{ZPE}_{H_2})/k_B T] \tag{5}$$

where the partition function for the gas phase molecule X_2 is

$$Q_{X_2}(T) = \sum_{J_{even}} (2J+1) e^{-\frac{\hbar^2 J(J+1)}{2 I_{X_2} k_B T}} \tag{6}$$

and we have assumed that the nuclear spins are coupled together to give a singlet spin state ($I = 0$), so that rotational states with odd J are not allowed in the gas phase. In Equation 6, I_{X_2} is the inertia moment of the diatomic molecule X_2, k_B is the Boltzmann's constant, while $\hbar = h/(2\pi)$ as usual. Notice that to obtain Equation 5, differently from what discussed previously,[13] we have assumed that thermal vibrational excitations of both gas phase diatomics and dissociatively adsorbed species contribute negligibly to the partition functions and, hence, to the definition of the selectivity coefficient. The fact that the latter is, indeed, a sensible approximation is well supported by the harmonic vibrational frequencies for all species involved, which we found to be well in excess of 600 cm^{-1} (i.e. whose Einstein's

temperature is roughly $\vartheta_E = h\nu/k_B = 940$ K) even in the case of the least constrained motion (i.e. H^- bending on SrO). In principle, a similar reasoning could be carried out also with respect to the rotational partition function of gas phase diatomics simplifying Equation 5 (the $J = 0 \rightarrow 2$ gaps for H_2 and T_2 are, respectively, ~ 525 and 175 K, so that $Q(T) \simeq 1$ if T is low); we wish, however, to investigate also temperatures well above cryogenic ones (e.g. $T = 100$ K), a situation in which it may no longer be possible to neglect the contribution to $Q_{X_2}(T)$ due to thermal excitations when X = D or T (the relative population in the $J = 2$ level of T_2 compared to the ground state is ~ 0.869 at $T = 100$ K).

Equation 5 is conveniently derived from the Langmuir's adsorption isotherm, its low temperature ($T < \vartheta_E$) quantum Statistical Mechanics derivation indicating that:

$$\vartheta = \frac{p\chi(T)}{1 + \chi(T)p} \tag{7}$$

where ϑ is the fractional site coverage, p is the gas pressure (in bar), and

$$\chi(T) = \frac{\exp[-\Delta E_0^{ads}/(k_B T)]}{k_B T q_{rot}(T)} \left(\frac{2\pi\hbar^2}{m_{X_2} k_B T}\right)^{3/2}. \tag{8}$$

Notice that both Equations 5 and 7 are important when it comes to fully understand the separation process. In fact, it is easy to predict an increase in selectivity upon lowering the system temperature due to the presence of the exponential factor (whose argument is positive, as the zero point energy of the adsorbed X_2 species is lower than that of H_2) and of the faster decrease of the rotational partition function upon decreasing T for the heavier isotopes. Low temperature, however, certainly means higher process costs to cool the system and, potentially, a very low equilibrium vapor pressure for both gases. The latter fact signifies, in turn, that a nearly irreversible saturation of the active sites with adsorbed H_2 may be possible, especially at the initial stages of the chromatographic process when the molar fraction of the heavier isotopes is very low, unless ample temperature swings are imposed. In principle, such swings may also be exploited to separate isotopes in a "batch–

like" fashion approach by trapping the strongly adsorbed ones (i.e. the heavier ones) at an appropriate low temperature, releasing them subsequently by raising the temperature.

3 Results and discussion

3.1 Adsorption

3.1.1 MgO

Table 1 provides the results obtained for the adsorption energy of X_2 isotopologues and their X–X equilibrium distance (R_e(X–X)) on various sites of MgO. We begin noticing that R_e depends substantially on the adsorption site, and in particular on the coordination number of the least coordinated ion. Thus, R_e is, either, substantially unmodified compared to the gas phase situation (R_e^{gas} = 0.7439 Å) when X_2 is located on a flat surface ($Mg_{5C}O_{5C}$), or slightly elongated when deposed onto an edge ($Mg_{4C}O_{4C}$). Conversely, X_2 substantially elongates when adsorbed close to a vertex site ($Mg_{3C}O_{4C}$ and $Mg_{4C}O_{3C}$). Indeed, the site characterized by Mg3C as least coordinated ion induces a X–X distance 2.4 times the gas phase one; R_e is only slightly longer than twice the gas phase one if X_2 is adsorbed onto $Mg_{4C}O_{3C}$, instead. The latter data appear, thus, to indicate that X_2 is, at least partially, dissociated in the vicinity of a vertex site, a result that is in good agreement with previous works discussing H_2 adsorption on nanostructured or defective MgO,[54,57,58,62,64,65,89] as well as with the finding that basic alkali–earth oxides are capable of dehydrogenating primary and secondary alcohols to produce aldehydes and ketones.[67–71]

With respect to the energetics evidenced in Table 1, shown also in Figure 2 for 3C sites to facilitate perusal, we notice that there is some correlation between the adsorption site, hence with R_e, and the adsorption energy for the various isotopologues of H_2. Thus, ZPE–corrected adsorption energies on $Mg_{5C}O_{5C}$ are always positive independently of the isotope involved, R_e(X–X) being comparable with the gas phase structure. Obviously, a positive

E^{ads} indicates that X_2 does not adsorb on the site, the energetic component of the chemical potential favoring the gas phase species as it does entropy. This conclusion is solely due to the contribution of the ZPE of adsorbed species, which present five more vibrational modes (molecular libration and center of mass motion with respect to the site) that are not present in the gas phase.[12,13,90] A similar trend for E^{ads} versus the isotopic mass is also witnessed when the $Mg_{4C}O_{4C}$ site is involved; in this case, however, the change in electronic energy upon adsorption is sufficiently negative to allow E^{ads} for D_2 and T_2 to become negative, *de facto* suggesting the site to be potentially able to selectively adsorb heavy isotopologues, especially T_2, with E^{ads} being close in value to what previously obtained when ammonia clusters were used to mimic the surface of amorphous ammonia ice.[12,13,90] For the latter, $S(D_2/H_2) \simeq 5$ was estimated at 30 K in the vicinity of a surface adsorbed ammonia molecule.

Table 1: ZPE–corrected adsorption energies (in kcal/mol) of H_2, D_2, T_2 homodiatomics on different adsorption sites of MgO. The changes in electronic energy for the adsorption processes are also reported between parentheses in the column regarding the H_2 species.

Adsorption site	$E^{ads}_{H_2}$	$E^{ads}_{D_2}$	$E^{ads}_{T_2}$	R_e(X–X) (Å)
$Mg_{5C}O_{5C}$	0.56 (-0.12)	0.36	0.27	0.744
$Mg_{4C}O_{4C}$	0.61 (-1.53)	-0.02	-0.29	0.757
$Mg_{3C}O_{4C}$	-2.84 (-7.05)	-4.07	-4.62	1.785
$Mg_{4C}O_{3C}$	3.98 (0.55)	2.98	2.53	1.549

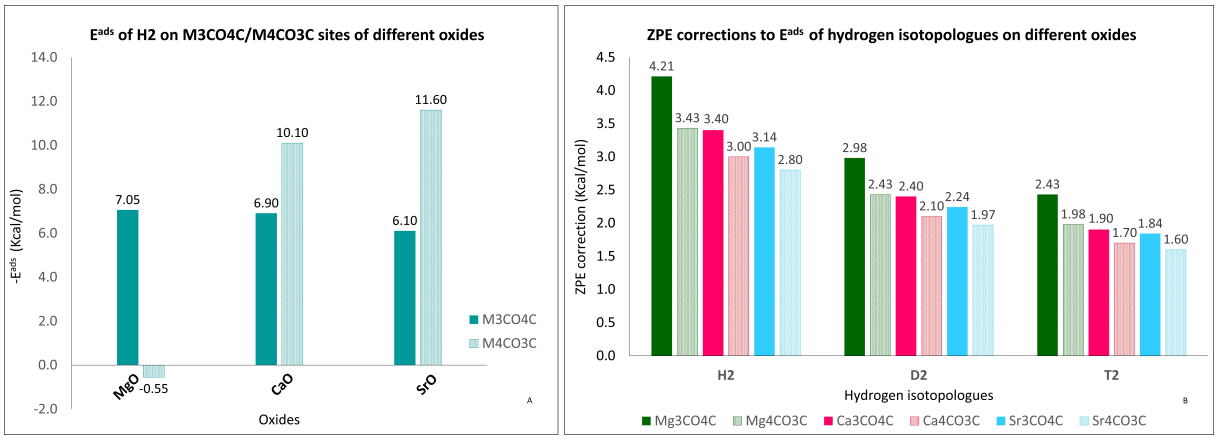

Figure 2: (Left) ZPE–corrected adsorption energetics for H_2 on 3C sites. (Right) ZPE–corrections of the adsorption energetics for X_2 on 3C sites.

At variance with what just discussed, the relative energetics for the adsorption on $Mg_{3C}O_{4C}$ and $Mg_{4C}O_{3C}$ appear somewhat more intricate in spite of their similar dissociative chemisorption, with the species adsorbed on the Mg3C site showing increasingly more negative adsorption energies upon increasing the isotope mass, while the results for the O3C site indicating that the gas phase molecule plus the cluster is the most stable state for this system. Focusing initially on the former site, it is interesting to notice that the different magnitude in the (negative) E^{ads} values related to $Mg_{3C}O_{4C}$ and $Mg_{4C}O_{4C}$ indicates that one should expect MgO nanoparticles to display two different temperatures for the onset of X_2 desorption,[14] the highest of which potentially being sufficiently high to allow for a less expensive quantum sieving based on this simple material.

Turning to the difference in behavior between the two vertex sites, this descends solely from a higher electronic energy (by roughly 7.6 kcal/mol) of the system with X_2 adsorbed on the O3C site. Somewhat anticipating results discussed in the following, we mention that a substantial part of such difference descends from a more negative adsorption energy of the hydride ion onto the Mg3C site compared to the Mg4C one,[54,57,58,60,62,64,65,89] which in not completely compensated by moving the proton site from O4C to O3C (see Table 2). Of course, we have verified the heterolytic bond dissociation via both Natural Bond Order analysis[91] and the partitioning of electron density *à la Bader*[92] (*vide infra* and Section 2 in the Supporting Information for further analysis details). Also important to mention, it is the fact that the electronic energy for the system with X_2 dissociated onto the O3C site is higher than its asymptotic value, a finding that suggests the presence of a transition state (TS) along the minimum path that brings the diatomic species onto the vertex site and that leads to dissociative chemisorption.

Bearing in mind the charged nature of the species adsorbed at either Mg3C or O3C sites,[54,57,58,60,62,64,65,89] it appears interesting that the equilibrium distance between H^+ and H^- varies according to the Mg site coordination number, the species with the lowest number of neighbour oxygen ions being the one with the longest separation. In turn, this

indicates that it is primarily the stabilization of the excess negative charge of the hydride that controls the H–H distance following chemisorption, the partial charge (hence, the local electric field or potential) of its adsorption site determining the availability of the hydride electronic cloud and, hence, the requirement for a stronger interaction with the coordinated proton. This rationalization is also supported by the relative distance between H^- from either Mg3C or Mg4C, the latter being roughly 0.12 Å longer (see also Reference[57]); a difference of 0.01 Å in distance is also seen between H^+ and O3C or O4C, the former being longer due to the "pull" that the hydride exerts on the proton itself rather than shorter due to the need for additional coordination by the O3C itself. All this discussion is supported by the optimized structures shown in Figure 3, where all important geometrical parameters are also reported.

From the viewpoint of the energetics indicated in Table 1, it appears that the adsorption close to a MgO vertex involves only small energy changes despite the fact that the heterolytic cleavage of H_2 would require nearly 399.9 kcal/mol to take place in the gas phase, as $E^{ZPE}_{H_2} \simeq$ –1.16456 hartree[93] and E_{H^-} = –0.5277 hartree.[94,95] As such, the driving force for the dissociative chemisorption ought to come from the coordination of the two products, H^+ and H^-, on their respective sites, and, at least to some extent, by their direct interaction once dissociated. To improve our understanding for this process, we calculated the ZPE–corrected adsorption energy for H^+ and H^- alone on the MgO model crystals, the results for these processes being reported in Table 2. Considering initially only the energy changes involving a single species adsorbing onto MgO, we notice that there is marked dependency of the latter values on the species involved (the values are substantially less negative for H^- than H^+), as well as the adsorption site involved whatever the species, the less coordinated sites presenting always more negative energy changes. While the dependency on the species is largely expected as H^+ is a bare proton, the latter effect may, alternatively, be view as related either to the presence of increasingly more intense electric fields (hence of more negative amounts of work carried out by the system while a species adsorbs) due to a less uniform distribution of the charge supplied by the neighbour counterions the lower

the site coordination, or to a partial charge of higher magnitude attributable to the latter as less ions of opposite charge sit in the immediate vicinity and are thus able to donate or attract electrons (depending on their charge sign). Obviously, which representation ought to be preferred is expected to largely depend on the specific process that is investigated, as in the case of hydride transfer to a carbonyl group[67–70] (also, *vide infra* the study of the possible reactivity induced by the dissociative adsorption on molecules in the gas phase).

As for the global adsorption process, it is immediately evident from the results reported in Table 2 that, taken separately, the adsorption energy for the two products does not suffice to drive the heterolytic dissociation; in fact, more than 90 kcal/mol are missing to justify the spontaneous nature of the process suggested by our structural optimizations. However, the Coulomb interaction between the products may substantially contribute to the systems' total energy in both the $Mg_{3C}O_{4C}$ and $Mg_{4C}O_{3C}$ cases, as clearly indicated by the data on the Coulomb point–like charges interaction reported in the last column of Table 2. Albeit the latter values are likely to be overestimated and one should also add the work required to distort the optimized geometries for the single species as well as the relaxation of the electron density due to their simultaneous presence to the total energy budget, it appears that there may be a sufficiently large contribution due to Coulomb interaction itself.[56] It thus seems that the energy lost by separating charges upon dissociation is largely recovered when species are co–adsorbed, and that the small adsorption energy values indicated previously are due to a nearly complete cancellation of large energetic effects.

Table 2: Vibrationally ZPE–corrected adsorption energies (in kcal/mol) of H^+ and H^- on different adsorption sites of MgO and their sum. The equivalent electrostatic interaction for two unit point charges at distance R_e when H_2 is dissociated (see Table 1) are also reported to facilitate the discussion.

Adsorption site	H^-	H^+	Sum	$-1/R_e$
$Mg_{5C}O_{5C}$	-22	-226	-248	
$Mg_{4C}O_{4C}$	-37	-227	-264	
$Mg_{3C}O_{4C}$	-79	-227	-306	-186.0
$Mg_{4C}O_{3C}$	-37	-267	-304	-214.3

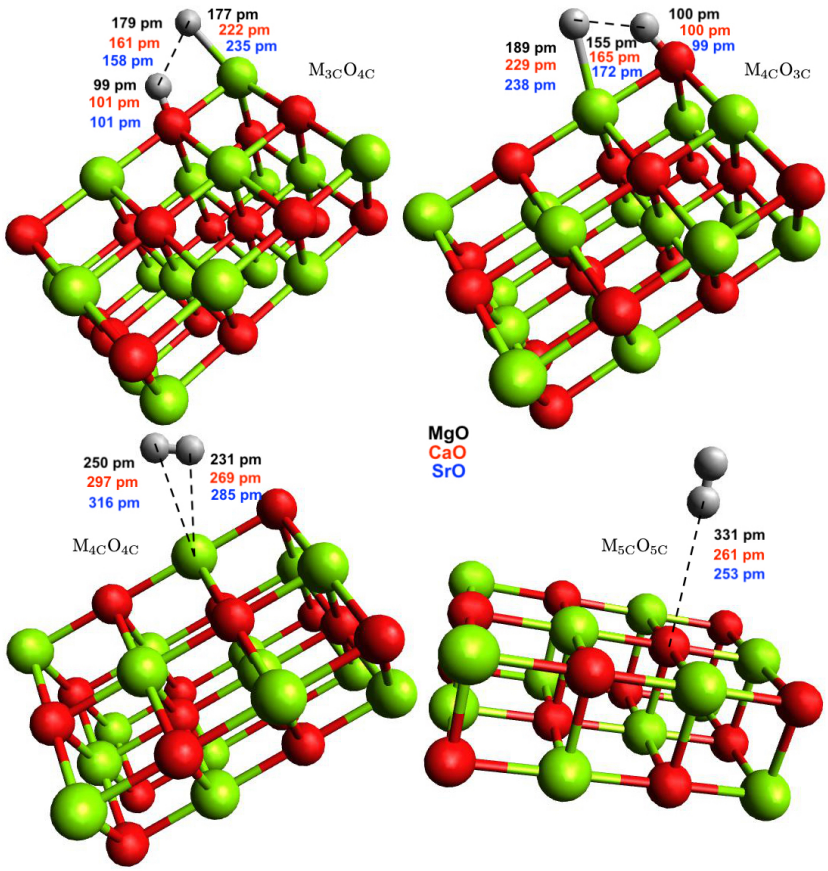

Figure 3: Equilibrium geometries for H_2 adsorbed onto MgO (color coding: Mg, green; O, red; H, grey); relevant distances are also provided (in pm) for CaO and SrO to highlight the impact of changes in the oxide electronic structure.

From the data collected in Table 1 for the $Mg_{3C}O_{4C}$, we have computed the theoretical low–pressure adsorption selectivities and $p_{vap} = 1/\chi(T)$ values as a function of the temperature using Equation 5 and the appropriate definitions; data for the alternative sites have not been generated as it makes little physical sense to estimate selectivities for non–adsorbing locations. The obtained result are shown in Figure 4. As it is easily noticed, theoretical selectivities for the heavier isotopes are quite high, being five times higher than the highest CAQS value recorded so far for the pair D_2/H_2 at T = 100 K in Cu(I)–exchanged zeolites.[14] Indeed, the dependence of $S(X_2/H_2)$ with respect to T^{-1} appears very close to exponential in nature, the fitting with an analytical relationship of the form $S = S_\infty \exp[-A/T]$ capturing a very high fraction of the data variance ($R^2 = 0.99999$). In turn, this finding indicates that

the prefactor $\frac{Q_{H_2}(T)}{Q_{X_2}(T)}$ in Equation 5 presents a much weaker dependence on the temperature than its exponential counterpart, which substantially dominates the temperature behaviour.

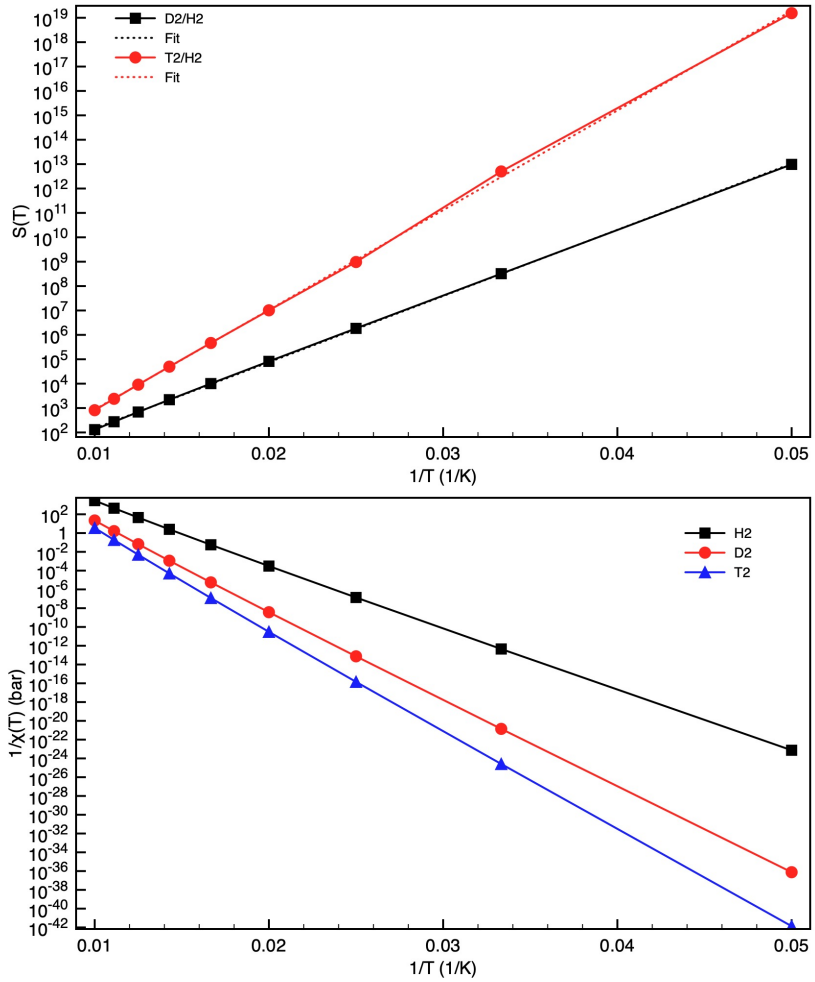

Figure 4: (Top) $S(D_2/H_2, T)$ and $S(T_2/H_2, T)$ for the chemisorption of X_2 onto $Mg_{3C}O_{4C}$. The short dashed lines represent the results of data fitting with the function $S = S_\infty \exp(-A/T)$. (Bottom) Equilibrium pressure for half–coverage of $Mg_{3C}O_{4C}$ sites (p_{vap}).

As for $p_{vap} = 1/\chi(T)$ (see bottom panel of Figure 4), we notice a substantial exponential dependence of the latter quantity (representing the X_2 equilibrium gas pressure at which half of the Mg3C sites are saturated with adsorbed molecules) on T^{-1} in the range $T \in [20, 100]$ K, the rationale for the latter finding being coincident with the one proposed for $S(X_2/H_2)$ above. Indeed, the magnitude of p_{vap} appears very low, suggesting that all isotopologues are *de facto* strongly adsorbed, so that a larger isosteric heat of adsorption (e.g. as the

9.3/17.4 kcal/mol range found for Cu(I)−ZSM–5[14]) may not be needed. In fact, one may even consider the lower magnitude of the adsorption energy for MgO compared to the case of the zeolite (see also Refs.[96,97]) to be a "blessing in disguise", as it may be easier to select an operational temperature at which both the selectivity and the rate of desorption are most advantageous for the separation process. For instance, it may be possible to find a range of temperatures in which H_2 is *de facto* not or very weakly adsorbed, while D_2 is strongly adsorbed by the Mg3C sites.

Extending our comparison with the Cu(I)−ZSM–5 introduced above, we notice that the better selectivity indicated by our results for the Mg3C site compared to the zeolitic sites descends mostly from larger differences induced in the ZPE contribution to the adsorption energy upon increasing the isotope mass (see Fig. 2 for ZPE–corrections on 3C sites). Thus, the ZPE contribution to $E^{ZPE}_{H_2}$ is 1.23 kcal/mol higher than $E^{ZPE}_{D_2}$, which is again 0.55 kcal/mol higher than $E^{ZPE}_{T_2}$; the same differences are, at most, equal to 1.07 and 0.38 kcal/mol, respectively, for the zeolite system. As RT = 0.198 kcal/mol at T = 100 K, even a difference of 0.2 kcal/mol in adsorption energy may indeed nearly triple the selectivity toward D_2.

As the selectivity data may depend on the models and methods chosen, we have tested MgO energetics by relaxing the clusters, improving the theory levels, and comparing alternative cluster sizes. These results are respectively discussed in Sections 3, 4, and 5 of the Supporting Information, and they confirm the possible usage of MgO as solid chromatographic stationary phase, even though the energetic landscape is somewhat modified. In particular, the adsorption energy for the O3C site becomes substantially more negative, while the same quantity for the Mg3C site becomes more positive upon relaxation compared to the frozen model case. *De facto*, the O3C site becomes the strongest adsorber (by roughly 6 kcal/mol at the electronic energy level, *vide* Table 4 in the Supporting Information) between the 3C sites following relaxation, contemporarily improving its ability to selectively adsorb heavy species. In parallel, longer H–H distances (by roughly 0.2 and 0.27 Å, respectively) are ob-

tained employing relaxed Mg3C and O3C models, a finding suggesting that the role played by the electrostatic H^-–H^+ interactions in defining the final adsorption energy is somewhat reduced compared to the frozen models; this is also supported by the outward displacement of the 3C sites from their position in the relaxed pristine oxide (which features a slight inward displacement, see Figure 4 in the Supporting Information) following X_2 chemisorption.

With the theoretical results just discussed clearly supporting the usage of MgO nanocrystals as a stationary phase for H_2/X_2 separation, one may wonder if already available experimental data may be reinterpreted to support the general correctness of our predictions. Indeed, evidences on the practical suitability of MgO as CAQS material may be extracted from infrared (IR) spectroscopic studies[54,57] and Temperature Programmed Desorption (TPD) experiments,[63,66,73] each set of investigations shedding light on complementary details of the H_2 adsorption process on MgO. Thus, IR spectra supported by DFT calculations indicated that MgO active sites can be separated in two groups basing on the reversibility of the adsorption process as a function of the partial pressure of H_2 at room temperature (RT), the irreversible sites being characterized by the proton bound to an O3C species, H^- held via a multidentate (at least bi–) coordination to Mg4C and Mg5C species, and by a decrease in ZPE–corrected energy upon adsorption spanning the 17.8–36.9 kcal/mol range.[57] Sites involved in the reversible adsorption of hydrogen molecules, instead, feature monodentate coordination on vertex species (both Mg3C and O3C) and the vicinal edge ions (O4C and Mg4C, respectively), and much less negative adsorption energies (roughly 6.9 kcal/mol). Identical conclusions are also reached for a similar analysis carried out on Zn–doped MgO,[54] with the additional indication of irreversible adsorption on segregated Zn3C sites.

Turning to TPD experiments, these were run on MgO samples activated at different temperatures in the range 673–1123 K, the collected spectra of H_2 desorbing after de–gasing at 77 K accurately characterizing the differences in population and adsorption enthalpy for at least seven different sites.[73] The juxtaposition of the latter experiments with identical ones involving adsorption of D_2[66] allowed further characterization of the adsorption sites,

confirming reversible adsorption for both the isotopologues onto $Mg_{4C}O_{3C}$ and $Mg_{3C}O_{4C}$, together with a low barrier to be surmounted to form the chemisorbed species. Importantly, the latter observation well correlates with a theoretical analysis of the adsorption process carried out on $(MgO)_4$ by Morokuma *et al.*,[64] which suggested a low electronic energy barrier of roughly 2.0 kcal/mol.

Interestingly, the energetic barrier indicated by the isotopic adsorption experiments[66] seems to somewhat depend on the adsorption site involved (no comparison can be made with results in Reference[64] due to the size of the model crystal), the reversible ones (i.e. $Mg_{4C}O_{3C}$ and $Mg_{3C}O_{4C}$) suggesting that the one affording the weakest interaction with H_2 is the one that is most affected by an increase in temperature during adsorption. In our view, such experimental results well correlate with our theoretical data, which insinuated the presence of an entry barrier toward $Mg_{4C}O_{3C}$.

Among previous TPD experiments, those involving H_2, D_2 and HD turned out to be instrumental in defining additional key aspects of the adsorption process onto MgO. In particular:

1. TPD spectra obtained following adsorption of only H_2 or D_2 at room temperature and subsequent cooling at 77 K displayed an upward shift in the desorption onset and peak maximum for the deuterium dimer compared to the protium one by roughly 20 K independently of the binding site. In turn, this result indicates that D_2 is more strongly bound than H_2, a finding that our results indicate to be entirely due to the differences in ZPE (*vide supra* Table 1), as well as that the surface/gas phase partition constant for the deuterium dimer ought to be higher than for the protium dimer. This was demonstrated at 308 K measuring adsorption isotherms for each isotopomer, the measured low pressure selectivity equal to 1.43 ± 0.04[66] agreeing exceptionally well with the estimate provided by our fitted function reported in the top panel of Figure 4.

2. Experiments run with HD and measuring the relative population of the three possible

desorbed species indicated that isotopic scrambling between adsorbed ions is negligible, a results well supported by the strong interaction that ought to be present between H^+ and H^- sitting on vicinal sites in order to energetically justify the heterolytic dissociation (*vide* Table 2 and associated discussion). Obviously, the formation of either H_2 or D_2 from adsorbed HD would imply an isotopic exchange with non–dissociated species while, simultaneously, breaking the strong electrostatic H^+–H^- interaction, which by itself seems to account for, at least, 100 kcal/mol. In other words, species adsorbed in the vicinity of Mg3C or O3C sites conserve the same isotopic composition upon desorption, a feature that one would certainly conserve whatever material is employed for the separation. Incidentally, the latter characteristic appears to be a common trait for all sites, and we shall thus discuss further this important aspect in Section 3.2.

3. On the sites displaying reversible adsorption, the activation energy for the desorption appears markedly lower (roughly 1.2 ± 0.2 kcal/mol) for H_2 than for the deuterium analogue.[66] Albeit the latter value turns out to be in excellent agreement with the difference in adsorption energy for the two species in Table 1, the mentioned result can only be qualitatively compared with our desorption energies as the harmonic frequencies at the desorption transition state differ from the one for the gas phase species (however, *vide infra* Table 7 suggesting a 1.0 kcal/mol difference between the desorption barrier of D_2 and H_2). Nevertheless, it suggests that there is a sufficiently large difference between their adsorption energetics to justify the different ranges of temperature (190–211 K for H_2 or 229–250 K for D_2) at which the reversible sites release the molecules; in our view, this, observation *de facto*, allows one speculating on MgO separation ability.

3.1.2 CaO

The ZPE–corrected adsorption energy E^{ads} of the X_2 isotopologues on various sites of CaO are collected in Table 3 (see also Fig. 2 for 3C sites) along with the corresponding X–X

equilibrium distances (R_e(X–X)). Other relevant geometrical information can be found in Figure 3. As for the geometrical data, we begin noticing that the nature of the adsorption is clearly revealed by the X–X distances; thus, R_e(X–X) $\gg$ 1 Å for chemisorbed X_2, which can thus be considered as partially dissociated. Physisorption is revealed by R_e(X–X) close to the gas phase value (0.744 Å) and R_e(H–O) $>$ 2 Å.

As with MgO, the nature of the adsorption (if it is energetically advantageous) depends on the adsorption site, and in particular on the coordination number of the least coordinated ion. When X_2 is located on a crystal face ($Ca_{5C}O_{5C}$) or an edge ($Ca_{4C}O_{4C}$), it is not adsorbed by CaO. Well-defined physisorption minima present on the electronic-energy PES disappear once ZPE is taken into consideration. We have also found a chemisorbed species on $Ca_{4C}O_{4C}$; its electronic energy is, however, much higher than the one of the related physisorption minimum, indicating it as a metastable species.

A small physisorption minimum has been detected also when X_2 is close to a $Ca_{3C}O_{4C}$ (except for H_2) or $Ca_{4C}O_{3C}$ vertex site. If X_2 is able to surmount a few kcal/mol barrier, it becomes chemisorbed with a R_e(X–X) larger than twice the gas-phase value, a result that is in good agreement with previous works discussing H_2 adsorption on nanostructured or defective CaO.[54,57–59,61,62,98]

Table 3: ZPE–corrected adsorption energies (in kcal/mol) of H_2, D_2, T_2 homodiatomics on different adsorption sites of CaO.

Adsorption site	$E^{ads}_{H_2}$	$E^{ads}_{D_2}$	$E^{ads}_{T_2}$	R_e(H–H) (Å)
$Ca_{5C}O_{5C}$	1.0 (-0.5)	0.6	0.4	0.750
$Ca_{4C}O_{4C}$	0.8 (-1.2)	0.2	0.0	0.758
$Ca_{4C}O_{4C}$[a]	7.2 (5.3)	6.7	6.4	1.216
$Ca_{3C}O_{4C}$	-3.5 (-6.90)	-4.5	-5.0	1.608
$Ca_{4C}O_{3C}$	-7.1 (-10.1)	-8.0	-8.4	1.632

[a] Metastable chemisorbed species.

As expected, the adsorption energy values become more negative on increasing the molecular mass of X_2, and they are sufficiently different to suggest that the vertex sites are potentially able to selectively adsorb heavy isotopologues. Chemisorption at the $Ca_{4C}O_{3C}$ site is

stronger by 3.4 to 3.5 kcal/mol, mostly due to the ZPE contributions. Indeed, the electronic energy favors the $Ca_{4C}O_{3C}$ site by 3.2 kcal/mol but the ZPE difference amounts to 0.5, 0.3, and 0.2 kcal/mol for H_2, D_2, T_2, respectively.

Table 4: Vibrationally ZPE–corrected adsorption energies (in kcal/mol) of H^+ and H^- on different adsorption sites of CaO.

Adsorption site	H^-	H^+	Sum	$-1/R_e$
$Ca_{5C}O_{5C}$	-17	-224	-241	
$Ca_{4C}O_{4C}$	-16	-237	-253	
$Ca_{3C}O_{4C}$	-49	-237	-286	-205.1
$Ca_{4C}O_{3C}$	-16	-287	-303	-207.3

With respect to the available experimental information on H_2 adsorbed onto CaO,[59,61] we notice that our results for chemisorbed species well agree with the indication of chemisorbed H_2, and they display semi–quantitative features similar to the experimental data, namely a substantial decrease in the H^-–Ca stretching frequency compared to the H^-–Mg one ($\Delta\bar{\nu}_{exp}$ = 200–350 cm^{-1} versus $\Delta\bar{\nu}_{DFT}$ = 180 cm^{-1}). In parallel, the distances of the sorbed species from the lattice atoms involved are longer when X_2 is adsorbed onto CaO than onto MgO (i.e. they justify the softer bonds indicated by both theory and experiments), and the ZPE for the adsorbed H_2 on CaO (e.g. $ZPE_{CaO–H_2}$ = 9.8 kcal/mol on CaC3) is also decreased compared to the MgO case ($ZPE_{MgO–H_2}$ = 10.5 kcal/mol). The latter finding is indeed true for all isotopologues, the Hessian matrix evaluated at the PES minimum being identical for all X_2. At variance with what just discussed, the X–X distance in chemisorbed species appears to be shorter when the molecule is sorbed onto CaO by, at least, 0.1 Å. Indeed, we believe this finding to be a direct consequence of the softer bonds between the X species and the lattice ions when CaO is involved (this is true also for the $O-H^+$ bonds); as a result, also the harmonic vibrational mode that modifies the H^-–Ca–O–H^+ dihedral angle is somewhat higher in CaO than in MgO (i.e. $\Delta\bar{\nu}_{DFT} \simeq 60$ cm^{-1}).

Comparing the overall energetics for X_2 chemisorbed onto calcium and magnesium oxides, it is immediately apparent that the former more strongly binds the isotopologues independently of the adsorption site. The latter finding, as well as the relation with experimental

results, is confirmed by the additional tests discussed in the Supporting Information (see Sections 3, 4, and 5). The mentioned difference should be expected to impact on the fractional occupation of CaO when in equilibrium with gas phase X_2 increasing it substantially (*vide infra* for a quantitative comparison); however, experiments[61] seem to indicate that an overall similar behavior to the one seen for MgO with respect to reversible or irreversible adsorption ought to be expected. A more negative ZPE–corrected adsorption energy for X_2 onto CaO may, however, even be advantageous as it would shift upward the desorption temperature, potentially raising the operational temperature at which chromatographic separations could be carried out. Obviously, this may be expected to decrease operational costs, especially in term of the amount of energy required.

As for the source of the difference in the energetics of the two oxides, the latter appears multifaceted. In fact, it is mainly related to a higher proton affinity (hence, basicity) of CaO and to a more intense residual Coulomb interaction between the chemisorbed species[56] (see Table 4 for the adsorption energy of isolated H^+ and H^- on different adsorption sites of CaO, as well as the QTAIM results reported in Section 2 of the Supporting Information). The hydride affinity of CaO is, instead, always lower than for MgO owning to the stronger acidity of the smaller Mg^{2+} ion. Whether or not the latter aspect is of importance with respect to the possibility of isotope scrambling between adsorbed species ought to be verified (*vide infra* Section 3.2 for a relevant discussion).

Selectivities $S(X_2/H_2)$ at low pressure, as well as $p_{vap} = 1/\chi(T)$ values as a function of the temperature, are shown in Figure 5.

The selectivities for the adsorption of D_2 and T_2 compared to the protium molecule are quite high, the values at T = 100 K being $S(D_2/H_2) \simeq 43$ and 23 when adsorbed, respectively, on Ca3C and O3C; $S(T_2/H_2)$ are $\simeq 163$ and 63, instead. The effect of the more negative adsorption energies on CaO compared to MgO is also clearly visible from the relative values of the half–coverage equilibrium pressure in the bottom panel of Figure 3, the results indicating a pressure lower by, at least, a factor of 131 when the Ca3C site on CaO

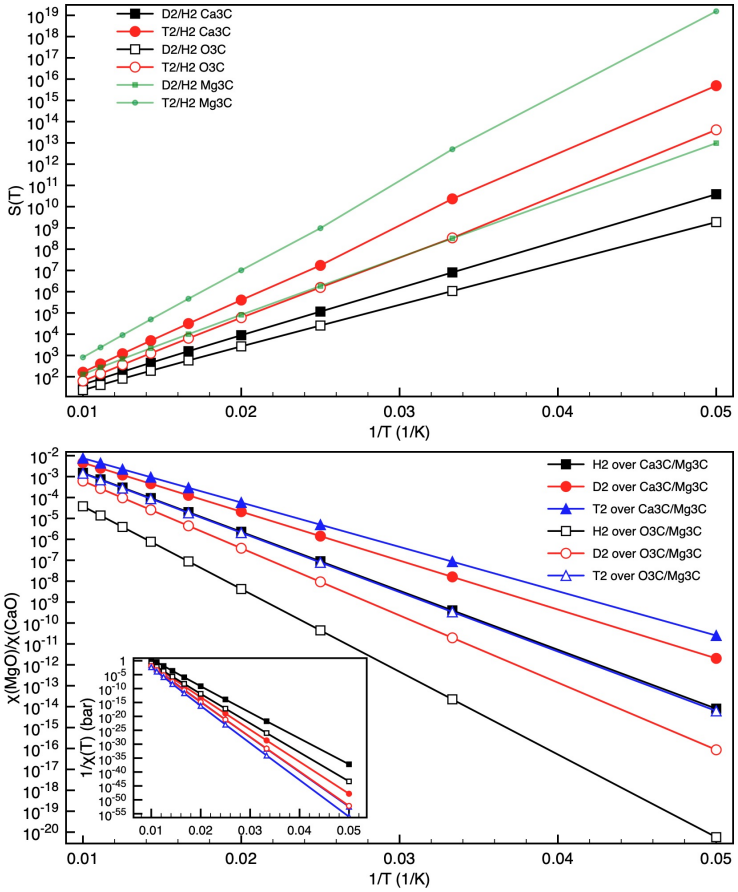

Figure 5: (Top) $S(D_2/H_2, T)$ and $S(T_2/H_2, T)$ for the chemisorption of X_2 onto $Ca_{3C}O_{4C}$ and $Ca_{4C}O_{3C}$. Results for $Mg_{3C}O_{4C}$ are also included for comparison. (Bottom) Ratio of the equilibrium pressure at half coverage for each one of the chemisorbed X_2 species on CaO with respect to MgO. Both Ca3C and O3C sites are considered for CaO, whereas only Mg3C is used for magnesium oxide. Half coverage pressure for CaO sites are shown in the inset.

is involved. The lower selectivities displayed by calcium oxide are easily rationalized by the less rapid decrease in the ZPE corrections on going from H_2, to D_2, and eventually to T_2 compared to the MgO case. The additional results related to the clusters' relaxation effect support identical conclusions (*vide* Supporting Information).

Despite what just mentioned, the selectivity of CaO with respect to the heavier isotopes still remains higher than or, at least, comparable with the selectivity at T = 100 K for Cu(I)−ZSM–5;[14] in practice, adsorption onto Ca3C is nearly twice as selective for D_2 than the most selective Cu(I) center in the zeolite, while the same quantity for O3C is less than 20% lower than found for Cu(I)−ZSM–5. Considering the economic cost of copper–related

substances compared to that of CaO, it may as well be that a separation on dispersed calcium oxide may remain competitive despite the results for the tricoordinated oxygen dianion. Besides, the adsorption energy on CaO for all isotopologues appears still less negative than the one on Cu(I)–exchanged zeolite as discussed earlier for MgO; thus, no difficulties with respect to the equilibration between gas phase species and the one adsorbed onto reversibly–adsorbing sites are expected.[61]

3.1.3 SrO

Table 5 and Figure 2 show the ZPE–corrected adsorption energies for the three isotopologues interacting with the various sites on SrO, together with their R_e(X–X). No or weak physisorption is suggested for the site with high coordination numbers (i.e. $Sr_{5C}O_{5C}$ and $Sr_{4C}O_{4C}$), E^{ads} decreasing in value upon decreasing the coordination number or increasing the isotope mass. A metastable chemisorbed structure was obtained for the $Sr_{4C}O_{4C}$ site; its E^{ads} is, however, positive (i.e. the species sits quite above the threshold for the separated SrO clusters and X_2), and the equilibrium X–X distance is quite shorter (namely, 1.246 Å) than any of the stable chemisorbed species discussed so far. Indeed, it is quite similar to the one obtained for the metastable chemisorbed species on $Ca_{4C}O_{4C}$ (*vide* Table 3).

Table 5: ZPE–corrected adsorption energies (in kcal/mol) of H_2, D_2, T_2 homodiatomics on different adsorption sites of SrO.

Adsorption site	$E^{ads}_{H_2}$	$E^{ads}_{D_2}$	$E^{ads}_{T_2}$	R_e(H–H) (Å)
$Sr_{5C}O_{5C}$	0.87 (-0.7)	0.41	0.20	0.751
$Sr_{4C}O_{4C}$	0.56 (-1.5)	-0.06	-0.33	0.760
$Sr_{4C}O_{4C}$[a]	6.23 (4.4)	5.70	5.46	1.246
$Sr_{3C}O_{4C}$	-2.96 (-6.1)	-3.86	-4.26	1.580
$Sr_{4C}O_{3C}$	-8.80 (-11.6)	-9.63	-10.0	1.723

[a] Metastable chemisorbed species.

As for the sites involving tricoordinated ions (i.e. O3C and Sr3C), we notice that both display a negative adsorption energy and quite long X–X distances, a clear indication of a chemisorptive process probably leading to the heterolytic dissociation of X_2; these conclusions

have been verified via QTAIM analysis and clusters relaxation (see Supporting Information). As for X–X equilibrium distances, it is interesting the fact that there is an inversion of relative values compared to similar sites on MgO; thus, this geometrical parameter is shorter when X_2 is adsorbed on the Sr3C site (1.580 Å) than on the O3C one (1.723 Å), while the same quantities are, respectively, 1.785 and 1.549 Å on MgO. Considering that $O-H^+$ distances do not vary substantially over all systems, we consider the inversion to be, again, a direct consequences of the interaction between the hydride ions and the strontium cation to which is bound. In general, the latter has a larger radius than the Mg cation and, thus, a longer equilibrium distance and and larger bond energy with anions. Its weaker electric field also polarizes H^- less strongly than when Mg cation were present, so that the electron density of the anion is more available to interact with the vicinal proton in the former case than in the latter. While the present discussion easily rationalizes the distances when a tricoordinated cation is involved, the inversion that is also present in case of O3C requires realizing that, in absence of a small and strongly polarizing cation, H^- has a more negative partial charge, the latter being hence more strongly repelled by the oxygen di–anion sitting at the vertex.

Turning to E^{ads} for the chemisorbed species, it is apparent that the latter are still following the trend already indicated for CaO, which suggested an inversion of the interaction strength between the two sites compared to magnesium oxide. In this case, the O3C site binds quite strongly all isotopologues, E^{ads} becoming of comparable magnitude with the weakest binding site characterized in Cu(I)–exchanged zeolites.[14] *Vice versa*, the Sr3C site appears even more weakly binding than Mg3C (see Table 1). This is clearly a result due more to the weaker interaction between the hydride with the Sr ion, as ZPE corrections are smaller for SrO (3.1 kcal/mol) than for MgO (4.2 kcal/mol). Further support for what just mentioned can be found from the vibrationally corrected adsorption energies for the isolated H^+ and H^- shown in Table 6, as well as from the QTAIM analysis.

Comparing initially the results for H^-, it is evident that: 1) the adsorption energy is less negative than in the MgO case (especially when $Sr_{4C}O_{4C}$ and $Sr_{3C}O_{4C}$ are involved),

Table 6: Vibrationally ZPE–corrected adsorption energies (in kcal/mol) of H^+ and H^- on different adsorption sites of SrO.

Adsorption site	H^-	H^+	Sum	$-1/R_e$
$Sr_{5C}O_{5C}$	-19	-256	-275	
$Sr_{4C}O_{4C}$[a]	-21	-271	-292	-266.5
$Sr_{3C}O_{4C}$	-51	-271	-322	-210.1
$Sr_{4C}O_{3C}$	-21	-308	-329	-192.7

[a] Metastable chemisorbed species.

while it is roughly comparable with what found for CaO. Conversely, the adsorption energy of H^+ on the various SrO sites is at least 30 kcal/mol more negative than for both MgO and CaO, this result being a direct indication of the more marked basicity for the heavier alkali–earth oxide. *De facto*, it is the latter quantity that drives the sum indicated in Table 6 to become more negative than for the other two oxides, especially in the case of the most strongly binding $Sr_{4C}O_{3C}$ site.

Turning to the selectivity and the gauge of the isotope–specific adsorption $p_{vap} = 1/\chi(T)$, the data in Table 5 allow one to easily conclude that:

1. a slightly lower selectivity ought to be expected for SrO compared to the other two oxides owing to a smaller differences in ZPE for the isotopes on the chemisorbing sites on strontium oxide. This amounts to 0.91 and 0.83 kcal/mol for the H_2/D_2 pair on, respectively, Sr3C and O3C, or 1.00 and 1.20 kcal/mol for the H_2/T_2 couple. The same quantities are 1.23 (H_2/D_2) and 1.78 (H_2/T_2) kcal/mol on Mg3C (*vide supra* Table 1 and Figure 2), 1.01 (H_2/D_2) and 1.46 (H_2/T_2) kcal/mol on Ca3C, and 1.00 (H_2/D_2) and 1.40 (H_2/T_2) kcal/mol on $Ca_{4C}O_{3C}$ (*vide supra* Table 3). Notice, however, that D_2 adsorption selectivities on the two SrO chemisorbing sites must be quite similar owing to very similar difference in ZPE for the two isotopes.

2. A much lower p_{vap} ought to be expected for all X_2 on $Sr_{4C}O_{3C}$ because of the more negative E^{ads}; the same quantity should instead be higher (or at least quite comparable when H_2 is adsorbed onto the tricoordinated Mg ion) for the remaining cases. *De facto*,

the difference in E^{ads} for the Sr3C and O3C sites is sufficiently large for them to behave quite differently with respect the fractional occupation as a function of the gas partial pressure. In other words, the O3C site should be expected to preferentially adsorb X_2 species until completely saturated, while Sr3C would become populated only if an excess of gas molecules remains.

The comments just made find confirmation from the results on the isotopic selectivity and $p_{vap} = 1/\chi(T)$ over SrO shown in Figure 6 (*vide* also Ref.[99]). This notwithstanding, selectivities on SrO still remains quite high, roughly of the same magnitude or slightly less than what found for the Cu(I)–exchanged zeolites. The p_{vap} versus T plot shows, instead, the vast difference in adsorption equilibrium between the basic site of SrO and Mg3C, while the relative values for Sr3C and Mg3C clearly display that a marked dependency on the specific isotope is present due to the change in relative values of the adsorption energies.

3.1.4 Adsorption Energy Decomposition

Tables 2, 4, and 6 report the adsorption energies associated with the adsorptions of a bare proton and a hydride on the surface of the oxides under investigation. These data show that, regardless the kind of reactive sites and oxide, the adsorption energy associated with the proton reacting with an oxygen site is significantly more negative (by around 200–250 Kcal/mol) compared to the one associated with the reaction of the hydride with a metal site. They also show that such energy considerably increases with the decrease of the site coordination and the increase of the metal atomic number, thus partially justifying the trend in adsorption energies of H_2 summarized in Tables 1, 3, and 5, and collectively suggesting that the principal factor determining the more or less favored thermodynamics is the basicity of the oxide; this increases following the same trend.

Being the analysis exploiting Tables 2, 4, and 6 based only on a two-body decomposition, we also exploited the highly accurate QTAIM method to partition the molecular space and improve our understanding. As expected, QTAIM appears to be able to reconstruct

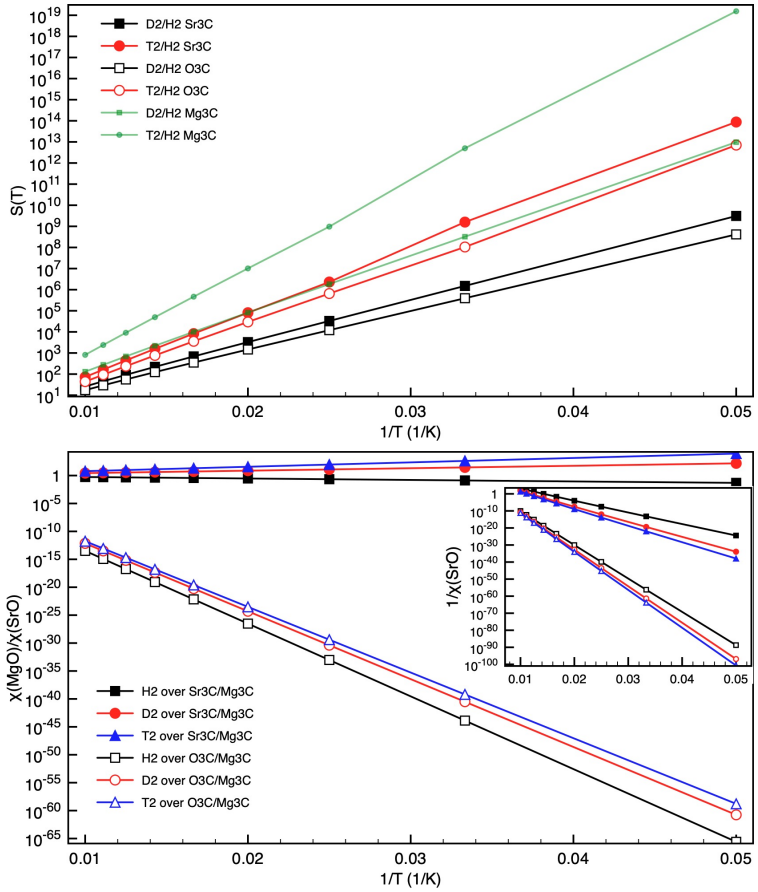

Figure 6: (Top) $S(D_2/H_2, T)$ and $S(T_2/H_2, T)$ for the chemisorption of X_2 onto $Sr_{3C}O_{4C}$ and $Sr_{4C}O_{3C}$. Results for $Mg_{3C}O_{4C}$ are also included for comparison. (Bottom) Ratio of the equilibrium pressure at half coverage for each one of the chemisorbed X_2 species on SrO with respect to MgO. Both Sr3C and O3C sites are considered for SrO, whereas only Mg3C is used for magnesium oxide. Half coverage pressure for SrO sites are shown in the inset.

the overall adsorption energetics with very good accuracy (see Table 1 in the Supporting Information). Thus, we also applied the latter method to computed atomic charges and delocalization indexes in order to characterize the strength and nature of the interactions between X_2 and reactive sites. For the sake of conciseness, the results of this in-depth investigation are widely discussed in Section 2.2 of the Supporting Information material. Instead, we report only those aspects which could not be evidenced discussing data in Tables 2, 4, and 6 in the following. Thus:

1. markedly exoenergetic contributions due to the coordination of H^+ and H^- on, respectively, O and M sites are partially contrasted by endoenergetic effects due to the

heterolytic bond breaking of X_2 and a response by the remaining cluster ions. The latter effects have opposite trends, competing among themselves in the definition of the most stabilizing site (see Figure 1 in the Supporting Information). Nonetheless, as discussed in Section 2.2 of the Supporting Information, they collectively allow to rationalize and justify the trend of the total adsorption energy of H_2 on different surface sites and oxides (Tables 1, 3, and 5).

2. While confirming that proton coordination to O^{2-} sites contributes the most in driving X_2 heterolytic chemisorption, the relative importance of the metal site increases more rapidly with the atomic number than for the oxide ones (see Figure 2 in the Supporting Information).

3. Partial charges and delocalization indexes indicate that the covalent nature of O-H bonds increases upon increasing the cation atomic number. Moreover, a significant difference exists between the M4C–H and the M3C–H bonds, the last of which showing a more marked covalent character in all cases. This phenomenon is however particularly enhanced in the MgO case, thus justifying a more favorable thermodynamics of the adsorption on $Mg_{3C}O_{4C}$ sites compared to $Mg_{4C}O_{3C}$ ones (see Table 2 in the Supporting Information).

3.2 Adsorption/Desorption Kinetics and Isotopic Scrambling

The electronic structure results discussed in Sections 3.1.1–3.1.3 and previous literature analysis[55,57,58,61,64–66,72] suggested the presence of entrance barriers for the heterolytic chemisorption of X_2 species. It thus appears interesting to evaluate the height of such barriers, especially in view of a selection of the most appropriate operational condition for the separation itself; Table 7 provide such data for H_2, with the metal oxide clusters ($M_{10}O_{10}$) and free diatomic molecules taken as energy zero; the same results are reported graphically in Figure 7. The same quantities for the heavier isotopologues are easily obtained scaling the

harmonic ZPE corrections by the appropriate mass factor. Importantly, we have selected to use a slightly smaller cluster size for the sake of computational efficiency. As we have discussed in Section 5 of the Supporting Information, the impact of changing the cluster size from $M_{10}O_{10}$ to $M_{16}O_{16}$ appears to be limited.

Table 7: ZPE–corrected entrance barrier for the chemisorption of H_2 (in kcal/mol) on the possible active sites with respect to isolated clusters and molecules. Differences in electronic energies are shown within brackets.

Adsorption site	H_2 adsorption	H_2 desorption
$Mg_{3C}O_{4C}$	4.1 (2.0)	4.9 (6.9)
$Mg_{4C}O_{3C}$	8.0 (6.7)	0.1 (2.1)
$Ca_{3C}O_{4C}$	0.7 (-1.0)[a]	4.9 (6.6)
$Ca_{4C}O_{3C}$	-0.3 (-1.7) [a]	4.4 (5.9)
$Sr_{3C}O_{4C}$	0.7 (-0.7)[b]	3.7 (5.4)
$Sr_{4C}O_{3C}$	1.8 (0.4)[b]	6.1 (7.4)

[a] The TS for the chemisorption of H_2 on both CaO sites is preceded by a physisorption minimum, which lie at 0.4 (–2.1) and –0.8 (–2.8) kcal/mol with respect to the common energy zero for Ca3C and O3C respectively.

[b] The TS for the chemisorption of H_2 on $Sr_{3C}O_{4C}$ is preceded by a physisorption minimum, which lie at 0.2 (–2.2) and –0.8 (–2.9) kcal/mol with respect to the common energy zero for Sr3C and O3C respectively.

As it can be seen, MgO presents always a positive entrance barrier, so that the adsorption on its vertex site ought to be considered activated. This is also true for the $Sr_{4C}O_{3C}$ site. Differently, the calcium oxide and the Sr3C site have TS's located below the electronic energy zero; in other words, the chemisorption should be considered more akin to a capture process, the incoming diatom possibly gathering enough energy to surmount the energetic barriers due to the attraction with the surface. In turn, the mentioned finding indicates that shallow physisorbed minima ought to be present, which we have localized at 0.4 (–2.1), –0.8 (–2.8), 0.2 (–2.2), and –0.8 (–2.9) kcal/mol below the ZPE–corrected (electronic) energy of the separated species for, respectively, Ca3C and O3C on CaO, and Sr3C and O3C on SrO. The latter data indicate that the effective chemisorption barriers are of the order of 1.1–3.3 kcal/mol with respect to the physisorbed species. *A posteriori*, we also optimized physisorbed X_2 on $Mg_{3C}O_{4C}$ and $Mg_{4C}O_{3C}$, as suggested by Morokuma and coworkers.[64,65] Even in this

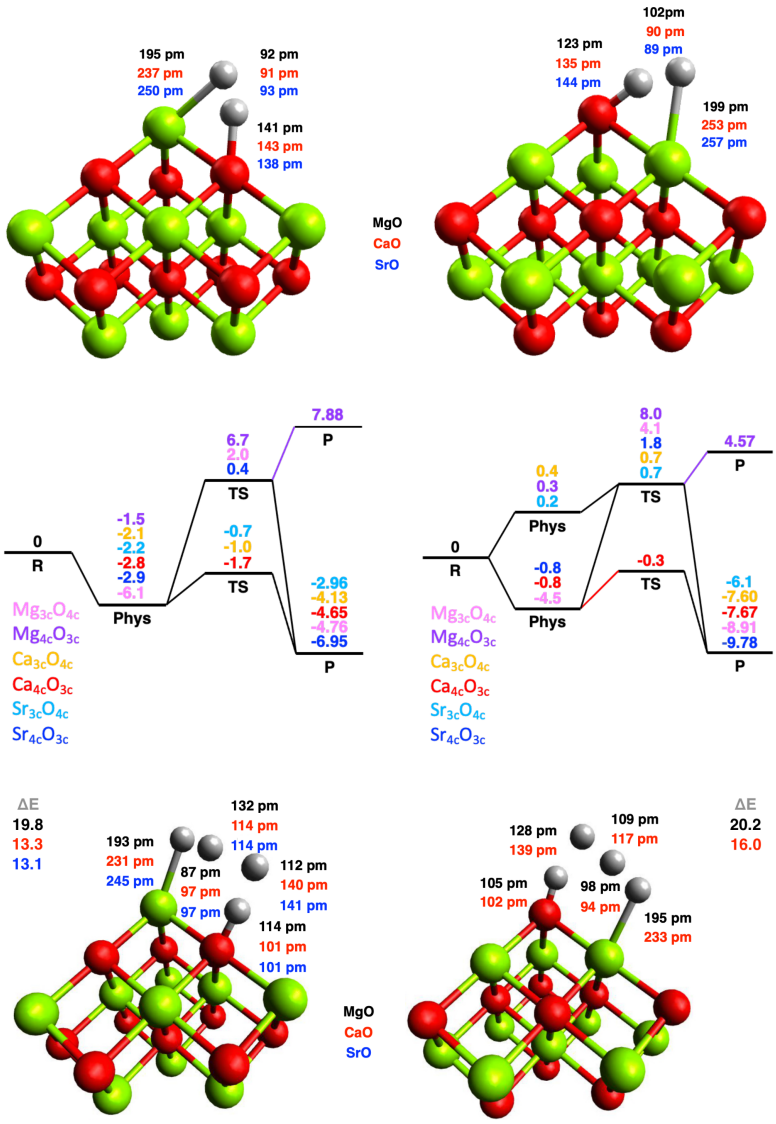

Figure 7: (Top) Optimized structure for the Transition State geometries leading to X_2 chemisorption on $M_{10}O_{10}$ models of the M3C and O3C sites; relevant distances are also indicated. (Middle) Electronic (left) and ZPE–corrected (right) energy profiles (in kcal/mol) for the chemisorption of H_2 on frozen M3C and O3C sites. Notice that physisorbed intermediates, which are minima on the electronic potential energy surface, may appear as non-bound due to the ZPE corrections. (Bottom) Transition state geometries and ZPE–corrected energies for the 4CE process involving a gas phase H_2 molecule colliding with a H_2 chemisorbed onto metal oxide vertex sites; relevant distances are also provided (in pm) for CaO and SrO to highlight the impact of changes in the oxides electronic structure.

cases, the physisorbed species lie below the electronic energy of the separated moieties by roughly –6.1 and –1.5 kcal/mol, respectively, our results being in very good agreement with

the data provided earlier on the Mg_4O_4 model.[64] The equivalent ZPE–corrected energies are –4.5 and 0.3 kcal/mol. In the end, all the presented energy results, albeit suggesting only a low adsorption energy, fully support the experimental evidences of a weak physisorption at low temperature (e.g. 70 K, at which RT = 0.14 kcal/mol) and of a reversible, albeit activated, chemisorption around room temperature (RT = 0.59 kcal/mol).[55,58,63,66,73]

As for the relevance to isotopic separation, we notice that ZPE corrections raise the entrance barriers compared to the mere electronic energy values; simultaneously, quantum vibrational effects lower the exit barrier. As a corollary, the ZPE–related increase of the entrance barrier is larger the lighter is the isotope, while the lowering of the exit barrier due to ZPE effects follows the order $T_2 < D_2 < H_2$; the rate of desorption should thus follow the same order, a conclusion supported by the results on MgO by Ito and coworkers,[66] whose experimental data suggested a ≈ 0.4 kcal/mol lower desorption barrier for H_2 than for D_2. Juxtaposing the lower entrance barrier for heavy isotopes due to ZPE effects with the 2.1 times higher chemisorption rate for H_2 than for D_2 found in Reference[63] suggests, however, that quantum tunnelling effects ought to be involved in defining the process rate. This conclusion is easily reached remembering that the relative collisional speed with the surface is only a factor $(\sqrt{2})^{-1}$ lower for the heavier isotope, a value that does not suffice to explain the substantially higher rate for H_2.

As last topic, it would be important to investigate the possible presence of alternative pernicious processes that may impair the separation effectiveness. For this reason, as well as in the attempt of shedding some light on contradicting experimental results suggesting that isotopic scrambling might[55] or might not[66] be possible, we investigated possible pathways leading to the production of (e.g.) HD from chemisorbed species interacting with gas phase molecules. At this stage, it is important to mention that previous computational works on the topic suggested that such scrambling might take place if a H_2 molecule is either heterolytically chemisorbed on extremely defective MgO sites and in the vicinity of a pre–chemisorbed D_2,[72] or vicinal to an adsorbed H atom[100] or a OH group that has survived the

calcination process. In those works, a barrier of twice the height (i.e. 7.6 kcal/mol[100]) of the ones we found for the chemisorption and desorption (namely 4.1 and 4.9 kcal/mol) was found for the reaction with the OH group, whereas nearly 60 kcal/mol appeared necessary to desorb HD from neighbouring chemisorbed pairs. Albeit the occurrence of such highly defective sites may not be vanishingly small (e.g. see Reference[57] for an atlas of possible surface defects probed via hydrogen chemisorption), the size of the structural models employed to investigate the scrambling processes was so small that we considered a reinvestigation employing larger clusters to be mandatory to improve our understanding of the title systems.

Alternative paths for the scrambling process involving the defective sites previously discussed for the hydrogen chemisorption were thus investigated. In particular, we selected to study the direct atom exchange (DAE) from a gas phase incoming molecule colliding with either H^+ or H^-, a choice motivated by knowing that gas phase collisions between H^- and H_2 lead to the atom substitution[95] and that H_3^+ is a stable species[101] easily leading to isotopic scrambling[102], and the concerted (heterolytic) splitting of the bond between the atoms of the incoming molecule and the formation of two molecular species with the chemisorbed H^+ and H^- in a four–center collisional exchange (4CE).[103]

As for DAE processes, we successfully obtained an atom exchange in both cases using adsorbed H–molecular H distance as reaction coordinate; the processes, however, have barriers in the range 35–45 kcal/mol depending on the surface species involved in the collision. Such energy requirements are clearly much larger than the one requested to desorb H_2 (7.05 kcal/mol) from the Mg3C site, a process that takes place already at relatively low temperature and that eliminates, *de facto*, the target species from the surface before DAE could take place.

Turning to 4CE, the transition state for such process at the Mg3C site of $Mg_{10}O_{10}$ was located at an electronic energy 19.8 kcal/mol above the separated species (see Fig. 7 for a representation) and with a quite high absolute value of the imaginary frequency, namely 1030 cm^{-1}. Barrier and imaginary frequency are even higher when the scrambling process

takes place on the O3C (i.e. 20.2 kcal/mol and 1557 cm^{-1}, respectively). Thus, also 4CE does not compete with the desorption of X_2 from the surface of MgO. This notwithstanding, the high TS imaginary frequencies hint at a possibly significant role of quantum tunneling in scrambling processes at low temperature. Similar conclusions can be drawn also for CaO and SrO. In fact, we found that the scrambling process must surmount an electronic energy barrier of 13.3 and 16.0 kcal/mol to take place on, respectively, the Ca3C and O3C sites in CaO. The barrier is instead around 13.1 kcal/mol when the Sr3C site in SrO is involved.

4 Conclusions

In the presented work, we have set to investigate whether or not simple and inexpensive alkali–earth oxides may provide suitable stationary phases for the chromatographic separation of hydrogen isotopes. This implies the possibility of selecting appropriate values for the partial pressure of gases and temperature so that the advancement of a inert carrier would separate two or more isotopes without trapping any of them on the stationary phase. We have tackled the task by theoretical means involving electronic structure calculations on model clusters to obtain the energetic data needed to predict adsorption isotherms and selectivities as a function of the temperature. Incidentally, we have provided the first quantitative estimates for the thermodynamics and kinetics of the processes involving H_2 and its isotopologues during their interaction with CaO and SrO. An in–depth analysis of the energetic aspects, supported also by a quantum topological analysis of electron density of our systems, indicated that more negative adsorption energies ought to be expected the heavier the metal cation is when the O3C site is involved; in other words, it follows the order of oxide basicity. In fact, adsorption thermodynamics goes from unfavorable to substantially spontaneous on going from Mg to Sr. In spite of this, all studied oxides feature markedly high selectivity toward the adsorption of heavy isotopologues, the latter quantity spanning the range from $\approx$ 15, for $Sr_{4C}O_{3C}$, to $\approx$ 150, for $Mg_{3C}O_{4C}$, for the competition between

D_2 and H_2 at 100 K. Interestingly, the temperature at which p_{vap} is sufficiently high to foster X_2 desorption appears to counter–correlate with oxide selectivity; this notwithstanding, the separation process still appears viable. Additional tests on the adsorption energetics reported in Sections 3, 4, and 5 support this conclusion.

Energy barriers in the reactive chemisorption channels appear low or non–existing with respect to separated species, so that heterolytically dissociated species can be easily generated. However, physisorbed intermediates appear to be possible at very low temperature, being located along the minimum energy path that connects gas phase X_2 with the chemisorbed counterparts. Finally, no isotopic scrambling due to the collision between gas phase molecules impinging on adsorbed species should take place even at room temperature, as suggested by the much higher energy barriers found for the latter process than for the molecular desorption.

From what discussed in this manuscript, it is evident that we have selected for our exploration a group of adsorption sites that are directly related to invariably present features of alkali–earth oxide nanocrystals, i.e. vertex, edges, and faces. Other possibilities are, however, available for MgO,[57,58,61,65,73,89,98,100] and we recall among these mono- and diatomic steps with or without kinks (producing bi– and tri–coordinating inverted corners and edges, together with vertexes), vicinal M3C–O3C sites, and divacancies. Albeit the relative number of such markedly defective sites may substantially depend on both the oxides preparation method and their post treatment,[58] it may be worth discussing what should be expected with respect to the separation efficiency if they were present. Importantly, kinks in mono– and bi–atomic steps seem to present a much more negative chemisorption energy than the site we investigated, with values spanning the range –36.9/–11.7 kcal/mol in the case of MgO.[57] As a change in adsorption energy ought to be expected to primarily impact on the desorption temperature, the mentioned sites should, hence, lead to the formation of either a very small amount of irreversible (with respect to the gas partial pressure) species if their presence is limited and the operating temperature is maintained sufficiently low, or being exploitable for

separation purposes at higher temperature. In the latter case, the ZPE corrections become important to define the site selectivity, the sites with the highest ZPE for the chemisorbed species being expected to be more selective toward heavier isotopes as the difference in ZPE scales proportionally to $1-\sqrt{m_H/m_X}$, and it is the latter differences that enters Equation 5. Comparing the relative values of stretching frequencies obtained in our work for H_2 on MgO chemisorption sites with the ones in Reference,[57] we notice that the latter tend to be higher by roughly 10–20%, leading to the conclusion that a higher selectivity ought to be expected. A similar comparison involving CaO and SrO cannot be carried out at the moment due to the lack of detailed information on the type and distribution of defective sites on the heavier oxides.

Finally, it is important to recall that not only selectivity per site is important for the practical use of a sieve, but also the total number of sites per volume or mass plays a role as enough adsorption locations ought to be present to allow the initially very D_2 or T_2–poor mixture to adsorb the heavy isotopes instead of the vastly more present hydrogen dimers. To show that nanosized oxides has the potential to be effective stationary phases, let us focus on MgO as is the most promising species recalling that the size distribution in Ref.[57] indicates an average cube size of 5 nm. As such, there are ca. $0.06/nm^3$ of either Mg3C or O3C sites located on the nanocrystal vertexes. ZSM-5, instead, contains $0.079/nm^3$ Al(III) sites, at least accordingly with the structure in Ref.[104] and the composition indicated in Ref.[14] Of the latter, 80% has been exchanged with Cu(II) ions and subsequently reduced to Cu(I), so that there are $0.065/nm^3$ adsorption locations. It thus appears that MgO may have, roughly, half of the zeolite sites, even though we have not included the defective sites discussed in the previous paragraph, which may be quite as much as the vertex locations and can be controlled by the preparation methods. If one assumes that nanostructured MgO is placed in contact with a D_2/H_2 mixture of total pressure p=1 bar and composition in D_2 equal to the natural abundance (i.e. 156 ppm) at a temperature of roughly 80 K, a straightforward application of the Langmuir's isotherm for the two isotopomers (see Figure 4

for the p_{vap} values) indicates that $\vartheta_{D_2}/\vartheta_{H_2} \simeq 0.108$, so that 10% of the Mg3C sites would be occupied by D_2. Importantly, even though Table 5 in the Supporting Information indicates that some adsorption strength on Mg3C is lost following relaxation and/or using a different theory level (i.e. p_{vap} increases), the activation of the O3C sites and their stronger binding suggests that an even lower operational pressure (roughly, by a few orders of magnitude according to B3LYP/6–311++G(2d,2p)/B3LYP/6–31++G(d,p) estimates in Table 5) could be used facilitating the process and reducing the costs. It thus seems that MgO, at least, may be consider a highly interesting candidate for the chromatographic separation of hydrogen isotopomers.

Acknowledgement

The Authors thank Dr. Davide Ceresoli for assistance and for making computing resources available to GB and AP.
SP, GB, and MM also thank Università degli Studi dell'Insubria for funding under the scheme Fondo Ateneo per la Ricerca (FAR–2022).

Supporting Information Available

The following file is available free of charge.

- main_SI.pdf: list of the coordinates for stationary points on the potential energy surface for the studied systems; additional details regarding the energy partitioning and electron density analysis, including a complete discussion of the QTAIM results; analysis of the energetic impact of adsorption sites relaxation; comparison of energetics obtained with different theory levels; size dependence of energetic quantities.

This material is available free of charge via the Internet at `http://pubs.acs.org/`.

References

(1) Iwai, Y.; Yamanishi, T.; O'hira, S.; Suzuki, T.; Shu, W.; Nishi, M. H-D-T cryogenic distillation experiments at TPL/JAERI in support of ITER. *Fusion Engineering and Design* **2002**, *61-62*, 553–560.

(2) Ducret, D.; Ballanger, A.; Steimetz, J.; Laquerbe, C.; Baudouin, O.; Sere Peyrigain, P. Hydrogen isotopes separation by thermal cycling absorption process. *Fusion Engineering and Design* **2001**, *58-59*, 417–421.

(3) Beenakker, J.; Borman, V.; Krylov, S. Molecular transport in subnanometer pores: zero-point energy, reduced dimensionality and quantum sieving. *Chemical Physics Letters* **1995**, *232*, 379–382.

(4) García-Arroyo, E.; Campos-Martínez, J.; Bartolomei, M.; Pirani, F.; Hernández, M. I. Molecular hydrogen isotope separation by a graphdiyne membrane: a quantum-mechanical study. *Phys. Chem. Chem. Phys.* **2022**, *24*, 15840–15850.

(5) Hernández, M. I.; Bartolomei, M.; Campos-Martínez, J. Helium Isotopes Quantum Sieving through Graphtriyne Membranes. *Nanomaterials* **2021**, *11*.

(6) Bhowmick, S.; Hernández, M. I.; Campos-Martínez, J.; Suleimanov, Y. V. Isotopic separation of helium through graphyne membranes: a ring polymer molecular dynamics study. *Phys. Chem. Chem. Phys.* **2021**, *23*, 18547–18557.

(7) Hu, S.; Gopinadhan, K.; Rakowski, A.; Neek-Amal, M.; Heine, T.; Grigorieva, I. V.; Haigh, S. J.; Peeters, F. M.; Geim, A. K.; Lozada-Hidalgo, M. Transport of hydrogen isotopes through interlayer spacing in van der Waals crystals. *Nature Nanotechnology* **2018**, *13*, 468–472.

(8) Lozada-Hidalgo, M.; Hu, S.; Marshall, O.; Mishchenko, A.; Grigorenko, A. N.;

Dryfe, R. A. W.; Radha, B.; Grigorieva, I. V.; Geim, A. K. Sieving hydrogen isotopes through two-dimensional crystals. *Science* **2016**, *351*, 68–70.

(9) Mella, M.; Curotto, E. Assessment of the Effects of Anisotropic Interactions among Hydrogen Molecules and Their Isotopologues: A Diffusion Monte Carlo Investigation of Gas Phase and Adsorbed Clusters. *The Journal of Physical Chemistry A* **2017**, *121*, 5005–5017.

(10) Curotto, E.; Mella, M. Diffusion Monte Carlo simulations of gas phase and adsorbed D2-(H2)n clusters. *The Journal of Chemical Physics* **2017**, *148*, 102315.

(11) Curotto, E.; Mella, M. Quantum Monte Carlo simulations of selected ammonia clusters (n=2-5): Isotope effects on the ground state of typical hydrogen bonded systems. *J. Chem. Phys.* **2010**, *133*, 214301.

(12) Mella, M.; Curotto, E. Quantum simulations of the hydrogen molecule on ammonia clusters. *J. Chem. Phys.* **2013**, *139*, 124319.

(13) Mella, M.; Curotto, E. Quest for inexpensive hydrogen isotopic fractionation: Do we need 2D quantum confining in porous materials or are rough surfaces enough? The case of ammonia nanoclusters. *J. Phys. Chem. A* **2016**, *120*, 8148–8159.

(14) Xiong, R.; Zhang, L.; Li, P.; Luo, W.; Tang, T.; Ao, B.; Sang, G.; Chen, C.; Yan, X.; Chen, J. et al. Highly effective hydrogen isotope separation through dihydrogen bond on Cu(I)-exchanged zeolites well above liquid nitrogen temperature. *Chemical Engineering Journal* **2020**, *391*, 123485.

(15) Hu, X.; Ding, F.; Xiong, R.; An, Y.; Feng, X.; Song, J.; Zhou, L.; Li, P.; Chen, C. Highly Effective H2/D2 Separation within the Stable Cu(I)Cu(II)-BTC: The Effect of Cu(I) Structure on Quantum Sieving. *ACS Applied Materials & Interfaces* **2023**, *15*, 3941–3952.

(16) Ha, J.; Jung, M.; Park, J.; Oh, H.; Moon, H. R. Thermodynamic Separation of Hydrogen Isotopes Using Hofmann-Type Metal–Organic Frameworks with High-Density Open Metal Sites. *ACS Applied Materials & Interfaces* **2022**, *14*, 30946–30951.

(17) Chen, X.; Liu, M.; Zhang, L.; Zhou, Y.; Ping, E.; Ding, C. New gas chromatographic packing ZIF-67@NH2–SiO2 for separation of hydrogen isotope H2/D2. *International Journal of Hydrogen Energy* **2021**, *46*, 13029–13037.

(18) Ping, E.; Ji, H.; Zhang, L.; Zhou, Y.; Ding, C.; Chen, X. Kinetic and chemical affinity quantum sieving effects of ZIF-67 for H2 and D2 and Gas chromatographic separation of hydrogen isotopes on columns packed with ZIF-67@NH2-γ-Al2O3. *ACS Applied Energy Materials* **2021**, *4*, 10857–10866.

(19) Ding, C.; Zhang, H.; Zhang, L.; Zhou, Y.; Ping, E.; Chen, X.; Kong, L. Hydrogen isotope separation on nickel-containing metal-organic framework@gama-alumina-based multicomponent composite packed column: Identification of individual role of each component. *Journal of Chromatography A* **2021**, *1660*.

(20) Li, L.; Ji, C.; Wang, W.; Wu, F.; Tan, Y.-X.; Yuan, D. The effect of pore sizes on D2/H2 separation conducted by MOF-74 analogues. *Inorganic Chemistry Frontiers* **2022**, *9*, 1674–1680.

(21) Yin, M.; Krishna, R.; Wang, W.; Yuan, D.; Fan, Y.; Feng, X.; Wang, L.; Luo, F. A [Th8Co8] Nanocage-Based Metal-Organic Framework with Extremely Narrow Window but Flexible Nature Enabling Dual-Sieving Effect for Both Isotope and Isomer Separation. *CCS Chemistry* **2022**, *4*, 1016–1027.

(22) Li, M.; An, Y.; Li, X.; Wang, X.; Zeng, N.; Chen, K.; Yao, W.; Song, J.; Chen, C.; Feng, X. et al. Quantitative analysis of hydrogen isotopes gas mixtures by cryogenic chromatography using low loading MOFs as stationary phase. *Microporous and Mesoporous Materials* **2021**, *312*.

(23) Li, X.; Wang, X.; Li, M.; Luo, J.; An, Y.; Li, P.; Song, J.; Chen, C.; Feng, X.; Wang, S. Highly selective adsorption of D2 from hydrogen isotopes mixture in a robust metal bistriazolate framework with open metal sites. *International Journal of Hydrogen Energy* **2020**, *45*, 21547–21554.

(24) Cao, D.; Ren, J.; Gong, Y.; Huang, H.; Fu, X.; Chang, M.; Chen, X.; Xiao, C.; Liu, D.; Yang, Q. et al. Quantum sieving of H2/D2 in MOFs: A study on the correlation between the separation performance, pore size and temperature. *Journal of Materials Chemistry A* **2020**, *8*, 6319–6327.

(25) Lee, S.; Oh, H. Hydrogen Isotope Separation by using Zeolitic lmidazolate Frameworks (ZIF-11). *Korean Journal of Materials Research* **2020**, *30*, 655–659.

(26) Han, G.; Gong, Y.; Huang, H.; Cao, D.; Chen, X.; Liu, D.; Zhong, C. Screening of Metal-Organic Frameworks for Highly Effective Hydrogen Isotope Separation by Quantum Sieving. *ACS Applied Materials and Interfaces* **2018**, *10*, 32128–32132.

(27) Yang, S.; Xie, H.; Zhu, H.; Zhang, L.; Zhou, Y.; Zhang, H.; Zhao, Z. Highly effective hydrogen isotope separation by cryogenic gas chromatography in a new stationary phase material MnCl2@CPL-1@γ-Al2O3. *International Journal of Hydrogen Energy* **2018**, *43*, 7973–7981.

(28) Cao, D.; Huang, H.; Lan, Y.; Chen, X.; Yang, Q.; Liu, D.; Gong, Y.; Xiao, C.; Zhong, C.; Peng, S. Ultrahigh effective H2/D2 separation in an ultramicroporous metal-organic framework material through quantum sieving. *Journal of Materials Chemistry A* **2018**, *6*, 19954–19959.

(29) Savchenko, I.; Mavrandonakis, A.; Heine, T.; Oh, H.; Teufel, J.; Hirscher, M. Hydrogen isotope separation in metal-organic frameworks: Kinetic or chemical affinity quantum-sieving? *Microporous and Mesoporous Materials* **2015**, *216*, 133–137.

(30) Oh, H.; Savchenko, I.; Mavrandonakis, A.; Heine, T.; Hirscher, M. Highly effective hydrogen isotope separation in nanoporous metal-organic frameworks with open metal sites: Direct measurement and theoretical analysis. *ACS Nano* **2014**, *8*, 761–770.

(31) Fitzgerald, S.; Pierce, C.; Rowsell, J.; Bloch, E.; Mason, J. Highly selective quantum sieving of D2 from H2 by a metal-organic framework as determined by gas manometry and infrared spectroscopy. *Journal of the American Chemical Society* **2013**, *135*, 9458–9464.

(32) Oh, H.; Park, K.; Kalidindi, S.; Fischer, R.; Hirscher, M. Quantum cryo-sieving for hydrogen isotope separation in microporous frameworks: An experimental study on the correlation between effective quantum sieving and pore size. *Journal of Materials Chemistry A* **2013**, *1*, 3244–3248.

(33) Li, J.-R.; Kuppler, R.; Zhou, H.-C. Selective gas adsorption and separation in metal-organic frameworks. *Chem. Soc. Rev.* **2009**, *38*, 1477–1504.

(34) Noguchi, D.; Tanaka, H.; Kondo, A.; Kajiro, H.; Noguchi, H.; Ohba, T.; Kanoh, H.; Kaneko, K. Quantum sieving effect of three-dimensional Cu-based organic framework for H2 and D2. *Journal of the American Chemical Society* **2008**, *130*, 6367–6372.

(35) Bezverkhyy, I.; Boyer, V.; Cabaud, C.; Bellat, J.-P. High Efficiency of Na- and Ca-Exchanged Chabazites in D2/H2 Separation by Quantum Sieving. *ACS Applied Materials & Interfaces* **2022**, *14*, 52738–52744.

(36) Xiong, R.; Chen, J.; Zhang, L.; Li, P.; Yan, X.; Song, Y.; Luo, W.; Tang, T.; Sang, G.; Hirscher, M. Hydrogen isotopes separation in Ag(I) exchanged ZSM-5 zeolite through strong chemical affinity quantum sieving. *Microporous and Mesoporous Materials* **2021**, *313*.

(37) Bezverkhyy, I.; Giraudet, M.; Dirand, C.; Macaud, M.; Bellat, J.-P. Enhancement of D2/H2Selectivity in Zeolite A through Partial Na-K Exchange: Single-Gas and

Coadsorption Studies at 45-77 K. *Journal of Physical Chemistry C* **2020**, *124*, 24756–24764.

(38) Bezverkhyy, I.; Pujol, Q.; Dirand, C.; Herbst, F.; Macaud, M.; Bellat, J.-P. D2 and H2 adsorption capacity and selectivity in CHA zeolites: Effect of Si/Al ratio, cationic composition and temperature. *Microporous and Mesoporous Materials* **2020**, *302*.

(39) Radola, B.; Bezverkhyy, I.; Simon, J.-M.; Salazar, J.; Macaud, M.; Bellat, J.-P. Enhanced quantum sieving of hydrogen isotopes: Via molecular rearrangement of the adsorbed phase in chabazite. *Chemical Communications* **2020**, *56*, 5564–5566.

(40) Perez-Carbajo, J.; Parra, J.; Ania, C.; Merkling, P.; Calero, S. Molecular Sieves for the Separation of Hydrogen Isotopes. *ACS Applied Materials and Interfaces* **2019**, *11*, 18833–18840.

(41) Giraudet, M.; Bezverkhyy, I.; Weber, G.; Dirand, C.; Macaud, M.; Bellat, J.-P. D2/H2 adsorption selectivity on FAU zeolites at 77.4 K: Influence of Si/Al ratio and cationic composition. *Microporous and Mesoporous Materials* **2018**, *270*, 211–219.

(42) He, D.; Zhang, L.; Liu, T.; Clowes, R.; Little, M. A.; Liu, M.; Hirscher, M.; Cooper, A. I. Hydrogen Isotope Separation Using a Metal–Organic Cage Built from Macrocycles. *Angewandte Chemie International Edition* **2022**, *61*, e202202450.

(43) Liu, M.; Zhang, L.; Little, M. A.; Kapil, V.; Ceriotti, M.; Yang, S.; Ding, L.; Holden, D. L.; Balderas-Xicohténcatl, R.; He, D. et al. Barely porous organic cages for hydrogen isotope separation. *Science* **2019**, *366*, 613–620.

(44) Jung, M.; Park, J.; Muhammad, R.; Kim, J. Y.; Grzimek, V.; Russina, M.; Moon, H. R.; Park, J. T.; Oh, H. Elucidation of Diffusivity of Hydrogen Isotopes in Flexible MOFs by Quasi-Elastic Neutron Scattering. *Advanced Materials* **2021**, *33*, 2007412.

(45) Qazvini, O.; Scott, V.-J.; Bondorf, L.; Ducamp, M.; Hirscher, M.; Coudert, F.-X.; Telfer, S. Flexibility of a Metal-Organic Framework Enhances Gas Separation and Enables Quantum Sieving. *Chemistry of Materials* **2021**, *33*, 8886–8894.

(46) Ju, Z.; El-Sayed, E.-S.; Yuan, D. Dynamic metal-organic frameworks for the separation of hydrogen isotopes. *Dalton Transactions* **2020**, *49*, 16617–16622.

(47) Mondal, S.; Kreuzer, A.; Behrens, K.; Schütz, G.; Holdt, H.-J.; Hirscher, M. Systematic Experimental Study on Quantum Sieving of Hydrogen Isotopes in Metal-Amide-Imidazolate Frameworks with narrow 1-D Channels. *ChemPhysChem* **2019**, *20*, 1311–1315.

(48) Oh, H.; Kalidindi, S.; Um, Y.; Bureekaew, S.; Schmid, R.; Fischer, R.; Hirscher, M. A cryogenically flexible covalent organic framework for efficient hydrogen isotope separation by quantum sieving. *Angewandte Chemie - International Edition* **2013**, *52*, 13219–13222.

(49) Chen, Y.; Bai, X.; Liu, D.; Fu, X.; Yang, Q. High-Throughput Computational Exploration of MOFs with Open Cu Sites for Adsorptive Separation of Hydrogen Isotopes. *ACS Applied Materials and Interfaces* **2022**, *14*, 24980–24991.

(50) Ha, J.; Jung, M.; Park, J.; Oh, H.; Moon, H. Thermodynamic Separation of Hydrogen Isotopes Using Hofmann-Type Metal-Organic Frameworks with High-Density Open Metal Sites. *ACS Applied Materials and Interfaces* **2022**, *14*, 30946–30951.

(51) Georgiev, P.; Drenchev, N.; Hadjiivanov, K.; Ollivier, J.; Unruh, T.; Albinati, A. Dynamics of bound states of dihydrogen at Cu(I) and Cu(II) species coordinated near one and two zeolite framework aluminium atoms: A combined sorption, INS, IR and DFT study. *International Journal of Hydrogen Energy* **2021**, *46*, 26897–26914.

(52) Kim, J.; Balderas-Xicohténcatl, R.; Zhang, L.; Kang, S.; Hirscher, M.; Oh, H.; Moon, H. Exploiting Diffusion Barrier and Chemical Affinity of Metal-Organic Frame-

works for Efficient Hydrogen Isotope Separation. *Journal of the American Chemical Society* **2017**, *139*, 15135–15141.

(53) Shi, H.; Yuan, H.; Li, Z.; Wang, W.; Li, Z.; Shao, X. Low-Temperature Heterolytic Adsorption of H2 on ZnO($10\bar{1}0$) Surface. *The Journal of Physical Chemistry C* **2019**, *123*, 13283–13287.

(54) Haque, F.; Finocchi, F.; Chenot, S.; Jupille, J.; Stankic, S. Site-Specific Hydrogen Reactivity of Zn0.05Mg0.95O Nanopowders. *The Journal of Physical Chemistry C* **2021**, *125*, 25841–25850.

(55) Ito, T.; Tominaga, N.; Tashiro, T.; Topi, K.; Ikemoto, I.; Kobayashi, H. Hydrogen isotope equilibration of HD on MgO below room temperature. *Bulletin of the Chemical Society of Japan* **1990**, *63*, 3016–3018.

(56) D'Ercole, A.; Pisani, C. Ab initio study of hydrogen dissociation at a surface divacancy on the (001) MgO surface. *The Journal of Chemical Physics* **1999**, *111*, 9743–9753.

(57) Haque, F.; Finocchi, F.; Chenot, S.; Jupille, J.; Stankic, S. Interplay between Single and Cooperative H2 Adsorption in the Saturation of Defect Sites at MgO Nanocubes. *The Journal of Physical Chemistry C* **2018**, *122*, 17738–17747.

(58) Gribov, E. N.; Bertarione, S.; Scarano, D.; Lamberti, C.; Spoto, G.; Zecchina, A. Vibrational and Thermodynamic Properties of H2 Adsorbed on MgO in the 300-20 K Interval. *The Journal of Physical Chemistry B* **2004**, *108*, 16174–16186.

(59) Garrone, E.; Stone, F. S. Ultraviolet–visible reflectance studies of hydrogen adsorption and CO–H2 interaction at MgO and CaO surfaces. *J. Chem. Soc., Faraday Trans. 1* **1987**, *83*, 1237–1251.

(60) H. T. Chen, G. P., L. Giordano From Heterolytic to Homolytic H2 Dissociation on

Nanostructured MgO(001) Films As a Function of the Metal Support. *J. Phys. Chem.* **2013**, *117*, 10623–10629.

(61) S. Coluccia, G. G. C. M., F. Boccuzzi Infrared Study of Hydrogen Adsorption on MgO, CaO and SrO. *J. Chem. Soc.* **1982**, *78*, 2111–2119.

(62) M. Cavalleri, G. M. A. G. S. C. G. M., A. Pelmenschikov Dissociative Adsorption of H2 on Defect Sites on MgO: A Combined IR Spectroscopic and Quantum Chemical Study. *Studies in Surface Science and Catalysis* **2001**, *140*, 131–139.

(63) Ito, T.; Sekino, T.; Moriai, N.; Tokuda, T. Hydrogen adsorption on magnesium oxide powders. *J. Chem. Soc., Faraday Trans. 1* **1981**, *77*, 2181–2192.

(64) Sawabe, K.; Koga, N.; Morokuma, K.; Iwasawa, Y. An ab initio molecular orbital study on adsorption at the MgO surface. I. H2 chemisorption on the (MgO)4 cluster. *The Journal of Chemical Physics* **1992**, *97*, 6871–6879.

(65) Sawabe, K.; Koga, N.; Morokuma, K.; Iwasawa, Y. An ab initio molecular orbital study on adsorption at the MgO surface. II. Site dependence of hydrogen chemisorption on the (MgO)4,6,8 clusters. *The Journal of Chemical Physics* **1994**, *101*, 4819–4825.

(66) Ito, T.; Murakami, T.; Tokuda, T. Isotopic study of hydrogen adsorption on magnesium oxide powders. *J. Chem. Soc., Faraday Trans. 1* **1983**, *79*, 913–924.

(67) Chieregato, A.; Velasquez Ochoa, J.; Bandinelli, C.; Fornasari, G.; Cavani, F.; Mella, M. On the Chemistry of Ethanol on Basic Oxides: Revising Mechanisms and Intermediates in the Lebedev and Guerbet reactions. *ChemSusChem* **2015**, *8*, 377–388.

(68) Tabanelli, T.; Passeri, S.; Guidetti, S.; Cavani, F.; Lucarelli, C.; Cargnoni, F.; Mella, M. A cascade mechanism for a simple reaction: The gas-phase methylation of phenol with methanol. *Journal of Catalysis* **2019**, *370*, 447–460.

(69) Pasini, T.; Lolli, A.; Albonetti, S.; Cavani, F.; Mella, M. Methanol as a clean and efficient H-transfer reactant for carbonyl reduction: Scope, limitations, and reaction mechanism. *Journal of Catalysis* **2014**, *317*, 206–219.

(70) Gyngazova, M. S.; Grazia, L.; Lolli, A.; Innocenti, G.; Tabanelli, T.; Mella, M.; Albonetti, S.; Cavani, F. Mechanistic insights into the catalytic transfer hydrogenation of furfural with methanol and alkaline earth oxides. *Journal of Catalysis* **2019**, *372*, 61–73.

(71) Izzo, L.; Tabanelli, T.; Cavani, F.; Blair Vàsquez, P.; Lucarelli, C.; Mella, M. The competition between dehydrogenation and dehydration reactions for primary and secondary alcohols over gallia: unravelling the effects of molecular and electronic structure via a two-pronged theoretical/experimental approach. *Catal. Sci. Technol.* **2020**, *10*, 3433–3449.

(72) Kobayashi, H.; Yamaguchi, M.; Ito, T. Ab initio MO study on adsorption of a hydrogen molecule onto magnesium oxide (100) surface. *The Journal of Physical Chemistry* **1990**, *94*, 7206–7213.

(73) T. Ito, M. Y. T. T., M. Kuramoto Active Sites for Hydrogen Adsorption on Magnesium Oxide. *J. Phys. Chem* **1983**, *87*, 4411–4416.

(74) Frisch, M. J.; Trucks, G. W.; Schlegel, H. B.; Scuseria, G. E.; Robb, M. A.; Cheeseman, J. R.; Scalmani, G.; Barone, V.; Petersson, G. A.; Nakatsuji, H. et al. Gaussian 09 Revision B.01. 2010; Gaussian Inc. Wallingford CT.

(75) Frisch, M. J.; Trucks, G. W.; Schlegel, H. B.; Scuseria, G. E.; Robb, M. A.; Cheeseman, J. R.; Scalmani, G.; Barone, V.; Petersson, G. A.; Nakatsuji, H. et al. Gaussian 16 Revision C.01. 2016; Gaussian Inc. Wallingford CT.

(76) Becke, A. D. Density-functional thermochemistry. III. The role of exact exchange. *The Journal of Chemical Physics* **1993**, *98*, 5648–5652.

(77) Stephens, P. J.; Devlin, F. J.; Chabalowski, C. F.; Frisch, M. J. Ab Initio Calculation of Vibrational Absorption and Circular Dichroism Spectra Using Density Functional Force Fields. *The Journal of Physical Chemistry* **1994**, *98*, 11623–11627.

(78) Izzo, L.; Mella, M. Interpreting "Acidity" as a Global Property Controlling Comonomer Reactivity in Olefin Polymerization. *Organometallics* **2013**, *32*, 3192–3202.

(79) Mella, M.; Izzo, L.; Capacchione, C. Role of the Metal Center in the Ethylene Polymerization Promoted by Group 4 Complexes Supported by a Tetradentate [OSSO]-Type Bis(phenolato) Ligand. *ACS Catalysis* **2011**, *1*, 1460–1468.

(80) Vigliotta, G.; Mella, M.; Rega, D.; Izzo, L. Modulating Antimicrobial Activity by Synthesis: Dendritic Copolymers Based on Nonquaternized 2-(Dimethylamino)ethyl Methacrylate by Cu-Mediated ATRP. *Biomacromolecules* **2012**, *13*, 833–841.

(81) Matrella, S.; Vitiello, C.; Mella, M.; Vigliotta, G.; Izzo, L. The Role of Charge Density and Hydrophobicity on the Biocidal Properties of Self-Protonable Polymeric Materials. *Macromolecular Bioscience* **2015**, *15*, 927–940.

(82) Amendola, V.; Bergamaschi, G.; Boiocchi, M.; Fusco, N.; La Rocca, M. V.; Linati, L.; Lo Presti, E.; Mella, M.; Metrangolo, P.; Miljkovic, A. Novel hydrogen- and halogen-bonding anion receptors based on 3-iodopyridinium units. *RSC Adv.* **2016**, *6*, 67540–67549.

(83) Mella, M. Exploring unvisited regions to investigate solution properties: The backyard of H3O+ and its aggregates. *Chemical Physics Letters* **2013**, *555*, 51–56.

(84) Tabanelli, T.; Cocchi, S.; Gumina, B.; Izzo, L.; Mella, M.; Passeri, S.; Cavani, F.; Lucarelli, C.; Schütz, J.; Bonrath, W. et al. Mg/Ga mixed-oxide catalysts for phenol methylation: Outstanding performance in 2,4,6-trimethylphenol synthesis with co-feeding of water. *Applied Catalysis A: General* **2018**, *552*, 86–97.

(85) Verbraeken, M. C.; Suard, E.; Irvine, J. T. S. Structural and electrical properties of calcium and strontium hydrides. *J. Mater. Chem.* **2009**, *19*, 2766–2770.

(86) Bashir, J.; Khan, R. T. A.; Butt, N.; Heger, G. Thermal atomic displacement parameters of SrO. *Powder Diffraction* **2002**, *17*, 222 – 224.

(87) Bader, R. F. W. *Atoms in molecules: A quantum theory*; Clarendon Press, 2003.

(88) Lu, T.; Chen, F. Multiwfn: A multifunctional wavefunction analyzer. *Journal of Computational Chemistry* **2012**, *33*, 580–592.

(89) Sawabe, K.; Morokuma, K.; Iwasawa, Y. An ab initio molecular orbital study on adsorption at the MgO surface. III. Cooperativity of ionic adsorbates. *The Journal of Chemical Physics* **1994**, *101*, 7095–7100.

(90) Sheppleman Jr., J.; Smizaski, G.; Curotto, E.; Mella, M. An analytical potential energy model for ammonia-H_2 from first principle. *Chem. Phys. Lett.* **2012**, *535*, 49–55.

(91) WEINHOLD, F.; LANDIS, C. R. NATURAL BOND ORBITALS AND EXTENSIONS OF LOCALIZED BONDING CONCEPTS. *Chem. Educ. Res. Pract.* **2001**, *2*, 91–104.

(92) Bader, R. F. W. A quantum theory of molecular structure and its applications. *Chemical Reviews* **1991**, *91*, 893–928.

(93) Kolos, W.; Wolniewicz, L. Improved Theoretical Ground-State Energy of the Hydrogen Molecule. *The Journal of Chemical Physics* **1968**, *49*, 404–410.

(94) Hylleraas, E. A. Über den Grundterm der Zweielektronenprobleme von H^-, He, Li^+, Be^{2+} usw. *Zeitschrift für Physik* **1930**, *65*, 209–225.

(95) Ayouz, M.; Dulieu, O.; Guérout, R.; Robert, J.; Kokoouline, V. Potential energy and dipole moment surfaces of H_3^- molecule. *The Journal of Chemical Physics* **2010**, *132*, 194309.

(96) Altiparmak, I.; Karakaya, B.; Uner, D.; Ipek, B. H2 adsorption on Cu(I)-ZSM-5: Exploration of Cu(I)-exchange in solution. *International Journal of Hydrogen Energy* **2019**, *44*, 18866–18874, Selected Papers from the 3rd International Hydrogen Technologies Congress.

(97) Ipek, B.; Altiparmak, I. Remarkable isosteric heat of hydrogen adsorption on Cu(I)-exchanged SSZ-39. *International Journal of Hydrogen Energy* **2020**, *45*, 34972–34982, 4th International HYDROGEN TECHNOLOGIES Congress.

(98) D'Ercole, A.; Ferrari, A. M.; Pisani, C. On the role of electrostatics in the heterolytic splitting of covalent bonds at defective oxide surfaces. *The Journal of Chemical Physics* **2001**, *115*, 509–518.

(99) As for the selectivities at the highest temperature displayed, we report that $S(D_2/H_2) \simeq 26$ and $S(T_2/H_2) \simeq 73$ on Sr3C, while $S(D_2/H_2) \simeq 17$ and $S(T_2/H_2) \simeq 44$ on O3C; these data are all substantially lower than the same quantity for CaO (in the same order, 43, 163, 24, and 63).

(100) Fujioka, H.; Yamabe, S.; Yanagisawa, Y.; Matsumura, K.; Huzimura, R. Possibility of hydrogen-deuterium exchange at surface irregularities of MgO: An ab initio MO study. *Surface Science* **1985**, *149*, L53–L58.

(101) Jaquet, R.; Khoma, M. V. A systematic investigation of the ground state potential energy surface of H3+. *The Journal of Chemical Physics* **2012**, *136*, 154307.

(102) Tabti, E. A. A. S. A. L., M.; Ouaskit, S. Unimolecular Dissociation of $H\equiv_2 n\equiv_1$ Hydrogen Clusters: Measured Cross Sections and Theoretically Calculated Rate Constants. *World Journal of Condensed Matter Physics* **2013**, *3*, 207–215.

(103) Hernández, M. I.; Clary, D. C. Four-center reactions: A quantal model for H4. *The Journal of Chemical Physics* **1996**, *104*, 8413–8423.

(104) Grau-Crespo, R.; Acuay, E.; Ruiz-Salvador, A. R. A free energy minimisation study of the monoclinic–orthorhombic transition in MFI zeolite. *Chem. Commun.* **2002**, 2544–2545.

Graphical TOC Entry